DISCOVERING NOVEL PLATINUM STRUCTURES

Khanyisa Prudence Mabunda

Centre for Materials Engineering

Department of Mechanical Engineering

January 2013

A dissertation submitted to the University of Cape Town, in fulfilment of the degree of Master of Science in Engineering

PLAGIARISM

This dissertation is submitted to the University of Cape Town for the degree of Master of Science in Engineering. I therefore confirm that this is indeed my original work and such work has not been submitted before for any degree or examination.

Khanyisa Prudence Mabunda

ABSTRACT

The Pt_8Zr ordering transformation in Pt 11 at. % Zr alloys has been studied. The study included determination of the formation of the Pt_8Zr phase and its order/disorder transformation temperature (T_c). Electron diffraction patterns and dark field images were obtained from transmission electron microscopy to characterize the Pt_8Zr phase. Microhardness measurements and light microscopy were used to investigate the Pt_8Zr ordered phase and its effects on hardness and microstructure respectively.

The Pt_8Zr ordered phase was found to be present in the initial as-cast condition and in specimens heat treated up to a temperature of 1070 °C. This is consistent with the DSC measurements of T_c, determined to be 1068 °C. The nucleation of the ordered phase was found to be rapid at any temperature below T_c but the growth of this ordered phase was rather slow, probably due to inadequate vacancies present in the alloy. The domain size of the Pt_8Zr phase was found to be approximately 10 nm for specimens heat treated at 1000 °C for up to 600 hours.

The effect of heat treatment medium on the ordering transformation of the Pt_8V in Pt 11 at. % V was also studied. The two heat treatment media were 15 % hydrogen (85 % Argon by volume) and a vacuum atmosphere. Transmission electron microscopy, using electron diffraction and dark field images, was used to characterize the Pt_8V phase formed for each heat treatment medium. DSC measurements were used to analyse the transition temperature, and microhardness measurements and light microscopy were used to investigate the Pt_8V ordered phase and its effect on hardness and microstructure for both heat treatment media.

The size of ordered domains formed at elevated temperatures was similar for both heat treatment media. There was also no significant difference in the hardness results, microstructural analysis or DSC measurements, for different heat treatment media.

ACKNOWLEDGEMENTS

I would like to thank the following people for making it possible for me to complete this degree, without them, it would had been impossible.

My supervisor Professor C.I. Lang for being SUPER awesome, working with her has being one of the most amazing experience.

Penny Park-Ross, Dr Sarah George and Liezl Mathews for all their support and expertise throughout.

Professor R Knutsen for allowing me to be part of the masters programme.

The Electron Microscope Unit at UCT for being patient with me.

The Electron Microscope Unit at UWC for allowing me to utilise their equipment.

My family and friends who never gave up on me, especially my beloved mother.

The National Research Foundation for their financial support.

Most importantly, the Almighty God for enabling me to get this far.

LIST OF ABBREVIATIONS

TEM	transmission electron microscopy
SEM	scanning electron microscopy
DSC	differential scanning calorimetry
LRO	long range order
SRO	short range order
Fcc	face centred cubic
Bct	body centred cubic
Fct	face centred tetragonal
Bcc	body centred cubic
Hcp	hexagonal closed packed

TABLE OF CONTENTS

LIST OF TABLES

LIST OF FIGURES

1. INTRODUCTION

Ordering has been in the past found to improve the mechanical properties in platinum alloys [3]. The ordered structure formed which is dispersed in the disordered matrix, results in an increase in hardness of some platinum alloys. The kinetics of ordering and the enhancement of this kinetics are always of great interest. Hydrogen is used to investigate the ordering kinetics of Pt 11 at. % V alloy. Therefore, the importance of this current study includes experimentally producing the Pt_8Zr (ordered alloy) phase, determining its transformation temperature and investigating on how to enhance the kinetics of ordered phase formation thereby ultimately reducing time and cost.

A superlattice is formed when different types of atoms are perfectly arranged in a crystal structure [1]. This perfect arrangement of atoms is known as ordering. An alloy is considered to be disordered when the constituent elements are arranged in a random manner. For alloys in an ordered configuration, disorder becomes more likely as temperature increases. The temperature at which alloys transform from the ordered state to the disordered state is known as the transformation temperature (T_c).

An A_8B ordered structure can be formed when an element of group 4 to 6 is added to a host metal of group 10 in the periodic table, in the ratio 1:8. The Pt_8Zr phase has been predicted to exist up to an order/disorder temperature between 827 °C and 1027 °C, but although the transformation temperature for some A_8B structures has been experimentally determined, this is not the case for the Pt 11 at. % Zr alloy [2]. One of the objectives of this study is to confirm the existence of Pt_8Zr and investigate its order/disorder transformation temperature.

The platinum-vanadium system has been previously studied and the Pt 11 at. % V composition was shown to have a T_c of 810 ± 10 °C for the Pt_8V order/disorder transformation [3]. Hydrogen has been found to affect the phase transformations in other alloys [4,5,6,8] but the effect of hydrogen on the ordering kinetics of platinum alloys has not previously been reported. One of the objectives of this research is to determine the effect

that hydrogen has on the ordering transformations of A_8B alloys; the Pt 11 at. % V alloy is investigated as a mode A_8B system because the ordering transformation is well characterized.

This report consists of seven chapters. Chapter 2 gives an overview of the scientific literature for both the platinum-zirconium system and the platinum-vanadium system. It describes ordering transformations in solid solutions, types of ordering and ordered structures including the A_8B ordered structures; and finally, the effect of hydrogen on ordering. Chapter 3 gives a description of the experimental procedures followed in the research. Chapter 4 gives the experimental results obtained; Chapter 5 discusses the results obtained in Chapter 4. Chapter 6 presents the conclusions drawn from the study and Chapter 7 shows the recommendations made based on these conclusions.

2. LITERATURE REVIEW

2.1 Platinum and Platinum Alloys

Platinum belongs to a group known as the platinum group metals (PGMs), namely platinum, palladium, iridium, ruthenium, rhodium and osmium, with platinum and palladium being the most abundant of this group. The PGMs lie next to each other in the periodic table; they are part of the transition metals and are characterised by strong interatomic bonds which determine the physical properties and crystalline structure. Below is a table of the crystalline properties of platinum.

Table 2.1: Crystalline properties of platinum [16].

PROPERTY	VALUE
Group number	VIIIC
Crystal structure	FCC
Type of structure	Cu (Al)
Atomic spacing (Å)	2.769
Lattice spacing (Å)	3.916

The crystal structure of platinum is face-centred cubic (fcc) and it is expected to mix readily with other fcc metals. This is not always the case; e.g. a phase separation occurs when platinum reacts with palladium, which is also fcc. Differences in bond structure, ionisation energy and melting points can cause a miscibility gap. The higher the difference in the melting points, there more readily the alloy separates into two mutually saturated solid solutions. For example the difference in the melting points of iridium and palladium is large; hence a miscibility gap exists and extends up to nearly 1500˚C. Platinum and palladium have a small melting point difference, thus the solid solution formed shows only a small tendency to separate [9].

Platinum alloys typically possess high electrical resistivity and tensile strength; but alloying platinum can compromises its high oxidation resistance [16,9]. In the liquid state, platinum is compatible with other metals and produces no immiscible systems. However, in the solid state, platinum dissolves up to 50 at % of other metals but is less soluble in other metals [9]. At low temperatures, platinum based solid solutions tend to undergo ordering transformations thereby forming ordered structures [7].

2.2 Types of Ordering

There are two types of ordering transformations that can take place in an alloy, namely long range ordering (LRO) and short range ordering (SRO). Long range ordering occurs at temperatures below the critical ordering temperature (T_c) whereas short range ordering takes place below and above T_c [1].

2.2.1 Ordering Transformations in Solid Solutions

A substitutional alloy is considered to be disordered when the elements are arranged in a random manner in a solid solution. Conversely, an ordered alloy is one in which the atoms of each element are arranged on preferred lattice sites. Ordered alloys usually have lower symmetry compared to disordered alloys. The effect of ordering on mechanical properties affects ductility (as in the AuCu alloy) if the transformation is accompanied by a change in symmetry [4].

A crystal structure with a perfect (ordered) arrangement of atoms is called a superstructure or a superlattice [3]. These produce diffraction patterns that have additional Bragg reflections, due to new and larger spacings between particular planes that are absent in the disordered alloys. These extra reflections are referred to as superlattice reflections seen are in the diffraction patterns of ordered alloys [11].

Kurnakov *et al.* [12] first deduced, from physical and mechanical properties measurements, the existence of the ordered structures Cu_3Au and CuAu in the gold-copper alloy system. Subsequently Bain [13], and Johansson and Linde [10], were the first to experimentally determine the presence of a superlattice; by means of diffraction of X-rays.

The formation of a superlattice usually occurs at relatively low temperatures and at stoichiometric compositions such as AB_3, AB or at compositions very close to stoichiometric compositions. The transformation temperature (T_c) separates a disordered phase from an ordered phase. Below T_c, the configuration of the atoms is ordered; above T_c the atoms are randomly arranged. As the temperature is decreased, order increases towards perfection. Figure 2.1 below shows disordered Cu 25 at. % Au and ordered (superlattice) Cu_3Au with the $L1_2$ designation. For the disordered phase the atoms are randomly arranged in the crystal structure but in the ordered phase the atoms occupy specific preferred sites; hence gold atoms occupy the "corners" and the copper atoms occupy the "faces" of the crystal structure shown. The ratio of gold to copper atoms remains at 1:3 according to the stoichiometric formula of Cu_3Au.

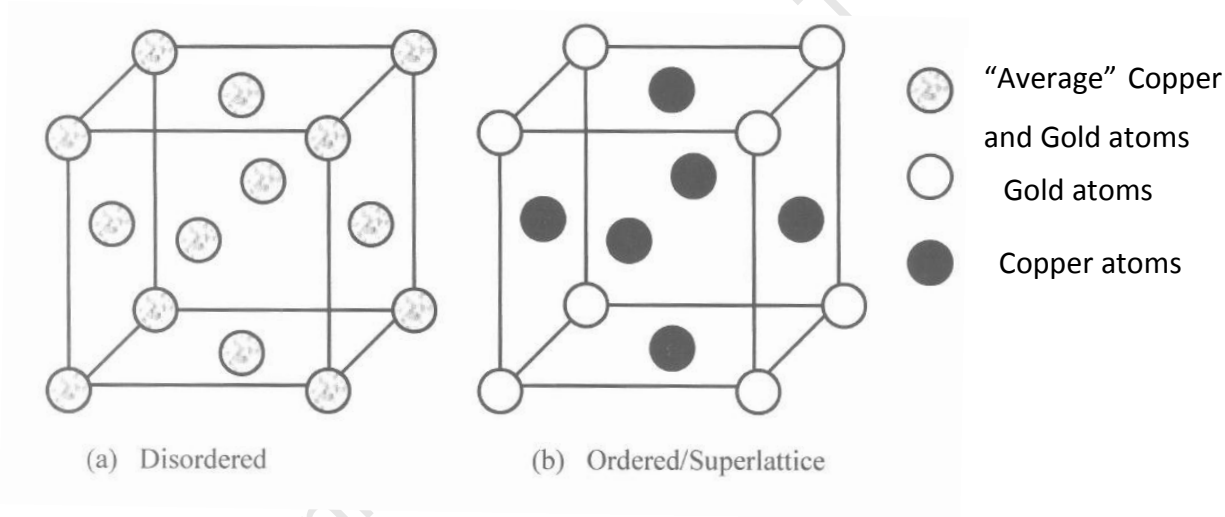

Figure 2.1: The disordered (A1) and superlattice ($L1_2$) structure of Cu_3Au (after Barrett and Massalski [14]).

On ordering, solid solutions do not necessarily change crystal structure owing to formation of a superlattice but may only reduce in symmetry. There are four such common ordered structure types namely (a) $L2_0$, (b) $L1_2$, (c) DO_{19} and (d) DO_3. These structures are illustrated in figure 2.2.

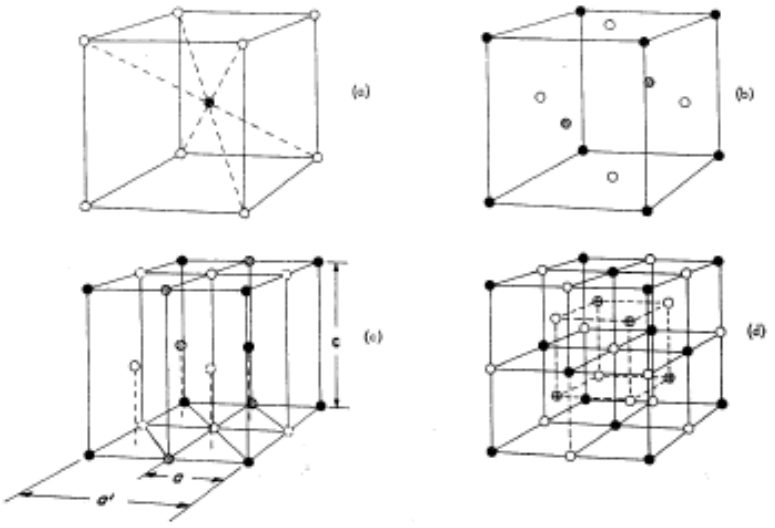

Figure 2.2: Common types of superlattices in which the crystal structure does not change upon formation of long-range order: (a) $L2_0$, (b) $L1_2$, (c) DO_{19}, (d) DO_3 (after Stoloff and Davies [15]).

The most frequently observed ordered lattice is the AB $L2_0$ type, referred to as B2 type. It is bcc in its disordered state, i.e. β type. Upon ordering the structure is said to form two interpenetrating simple cubic lattices, with all the A atoms on one sublattice and all the B atoms on the other sublattice as shown in figure 2.2(a). Figure 2.2(b) shows fcc Cu_3Au, figure 2.2(c) hcp Mg_3Cd and figure 2.2(d) bcc Fe_3Al, all with a general formula of A_3B. Four interpenetrating sublattices give the fcc $L1_2$ type (figure 2.2 (b)) which is the simplest of these three, as there is no change in unit cell size upon ordering. The DO_3 type (figure 2.2 (d)) is the most complex of the common superlattices, being built up of eight bcc unit cells, and may be thought of as being composed of four interpenetrating fcc lattices. The DO_{19} superlattice has the hcp crystal structure [15].

Table 2.2: Examples of the alloy types exhibiting the most common superlattices [15].

Structure type	Examples
$L2_o$	CuZn, FeCo, NiAl, CoAl, FeAl, AgMg
$L1_2$	Cu_3, Au_3Cu, Ni_3Mn, Ni_3Fe, Ni_3Al, Pt_3Fe
DO_{19}	Mg_3Cd, Cd_3Mg, Ti_3Al, Ni_3Sn
DO_3	Fe_3Al, Fe_3Si, Fe_3Be, Cu_3Al
$L1_0$	AuCu, CoPt, FePt, FePd

2.2.1.1 Short range ordering

Both short range and long range ordering can occur when the force of attraction between different atoms is stronger than the force of attraction between the same types of atoms. Short range order occurs both below and above T_c, and is characterised by short-range atomic correlations. Four models have been used to describe this type of ordering: statistical short range order, disperse short range order, microdomain short range order and the lattice defect model. These differ in homogeneity, heterogeneity and phase stability [36].

Short range order is measured by the parameter σ, which measures the extent to which, on average, each atom is surrounded by unlike neighbours relative to composition.

2.2.1.2 Long range ordering

When an alloy undergoes long range ordering, atoms arrange themselves in a regular pattern to form a superlattice. A long range ordered alloy occurs at or near a stoichiometric composition, often between transition metals which are on extreme ends of the periodic table [11].

Two types of long range ordering have been identified, based on their order-disorder transformation temperature: directly or permanently ordered alloys that retain long range ordering right up to the melting temperature with $T_c \geq$ Tm (melting point), and sequentially or reversibly ordered alloys that show long range ordering up to $T_c <$ Tm.

Compositional changes and temperature changes in alloys can cause deviation from perfect long range order. The degree of long range order is expressed by means of the Bragg-Williams parameter (S), as expressed in the equation 2.1 below [15].

$S = (p – r)/(1 – r)$ **Equation 2.1**

Where

S is the degree or extent of order

p is the probability that A atom sites are occupied by an A atom

r is the fraction of the total sites that are occupied by A atoms for perfect order

S varies from 1 to 0 (1 for complete order and 0 for complete disorder). The way in which the degree of order changes with temperature is dependent on the crystal structure. For example, when a fully ordered sample of an $L1_2$ or DO_{19} type alloy is heated up to T_c under nearly equilibrium conditions, S will decrease slowly from 1 to about 0.8. At T_c, S decreases discontinuously from 0.8 to 0, and at all temperatures above T_c, S is zero. Welber *et al.* [17] incorrectly concluded from specific heat measurements that Mg_3Cd disordered in a similar manner to β-brass, when in fact in the fully ordered region the degree of order of Mg_3Cd [18] only changes from 1 to about 0.8 in the same way as Cu_3Au.

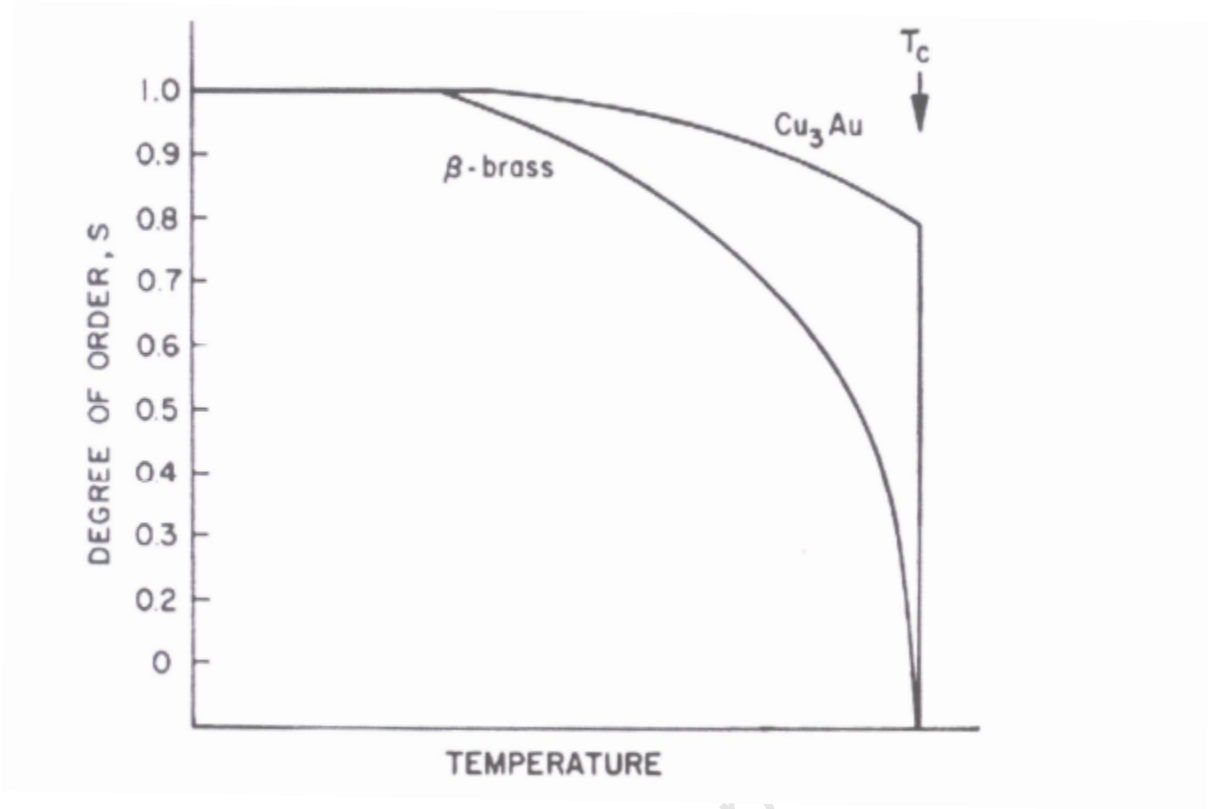

Figure 2.3: Variation of the degree of order with temperature for β-brass ($L2_0$ structure) and Cu_3Au ($L1_2$ structure), after Stoloff and Davies [15].

2.3 A_8B Platinum Alloys

An A_8B ordered structure occurs mostly when a solute element from group 4 to 6 is added to a group 10 host metal namely platinum, palladium or nickel [3]. Alloying platinum with an element from group 4 to 6 of the periodic table (Ti, Zr, Hf, V, Nb, Ta, Cr, Mo or W), a Pt_8X or A_8B ordered structure can be formed of which the prototype is Pt_8Ti. The Bravais lattice of the A_8B structure is bct. Even though all Pt_8X alloys appear to be thermodynamically stable, according to Ardell [2] they are kinetically slow to form, and a large amount of excess vacancies is required for the formation of the Ni_8X and Pd_8X phases. These vacancies can be produced either by rapid quenching or by charged-particle irradiation [2]. Taylor *et al.* [19] used a high-throughput method to computationally find 59 systems consisting of the A_8B phase, of which 48 are yet unobserved.

Corbel *et al.* [20] investigated the cold-rolled Pt 11.1 at. % V alloy to gain a better understanding of the incomplete transformation of the meta stable cubic disordered phase into the tetragonal ordered Pt_8V phase which had been earlier reported by Nxumalo and Lang [21]. The study showed that upon heating a disordered specimen above 450 °C, an ordering of vanadium atoms in the Pt 11 at % V alloy leads to the appearance of a tetragonal Pt_8V phase. Figure 2.4 illustrates the relationship between the single cubic structure of Pt as shown by the dashed line and the solid line which is the ordered tetragonal super-structure of the Pt_8Ti.

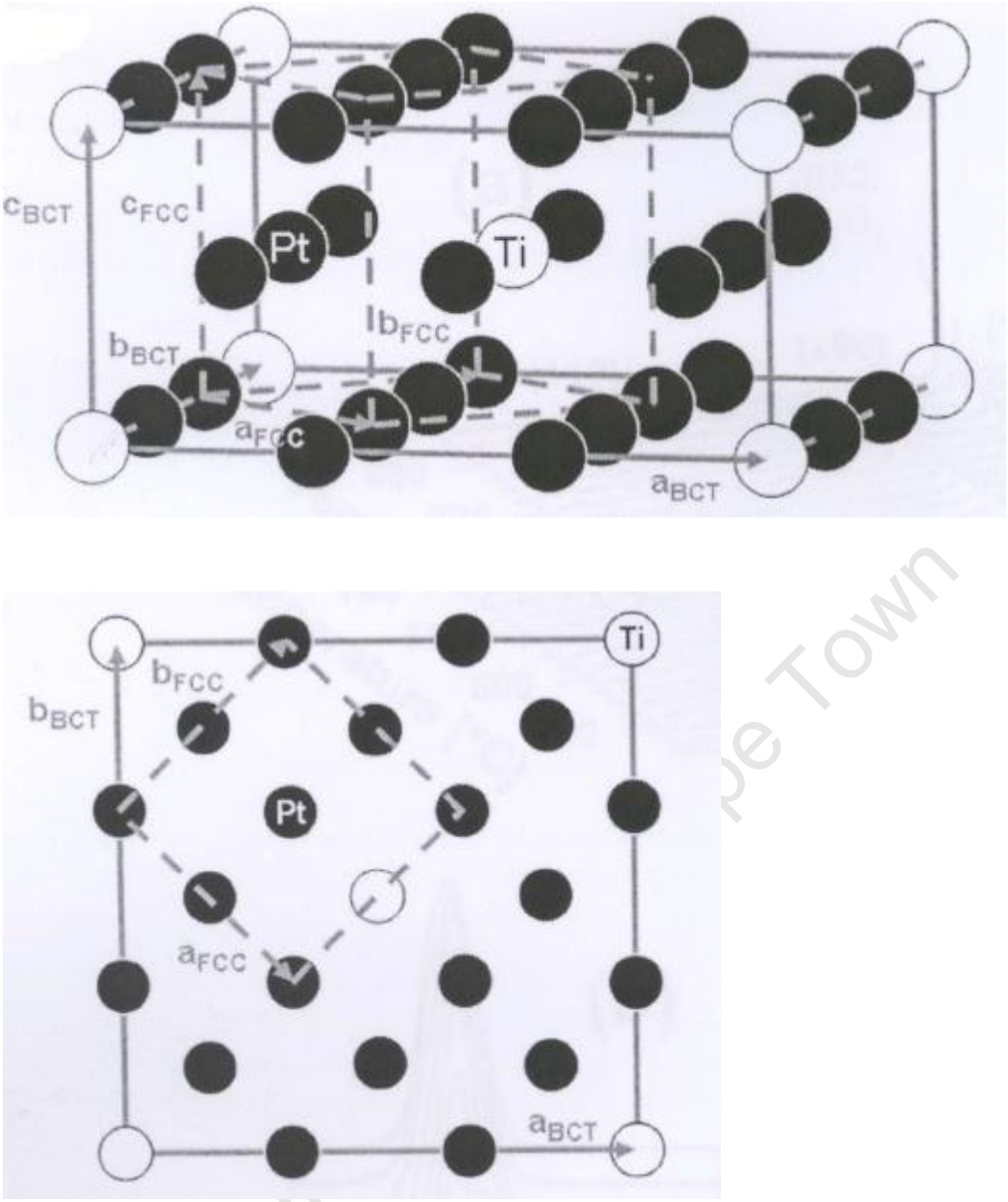

Figure 2.4: Change from simple cubic structure of Pt (fcc, space group Fm-3m no. 225) to the ordered tetragonal superstructure (bct, space group 14/mmm no. 139)) of Pt_8Ti. The dashed line illustrates the single cubic structure and the solid line illustrated the ordered tetragonal superstructure of Pt_8Ti (after Corbel *et al*. [20]).

Figure 2.5 shows an A_8B type superlattice after Quist *et al.* [22]. Although the ordered structure is body centred cubic (bct), in general it is described as face centred cubic (fct) for easy comparison with the face centred cubic (fcc) parent platinum [22,23,24].

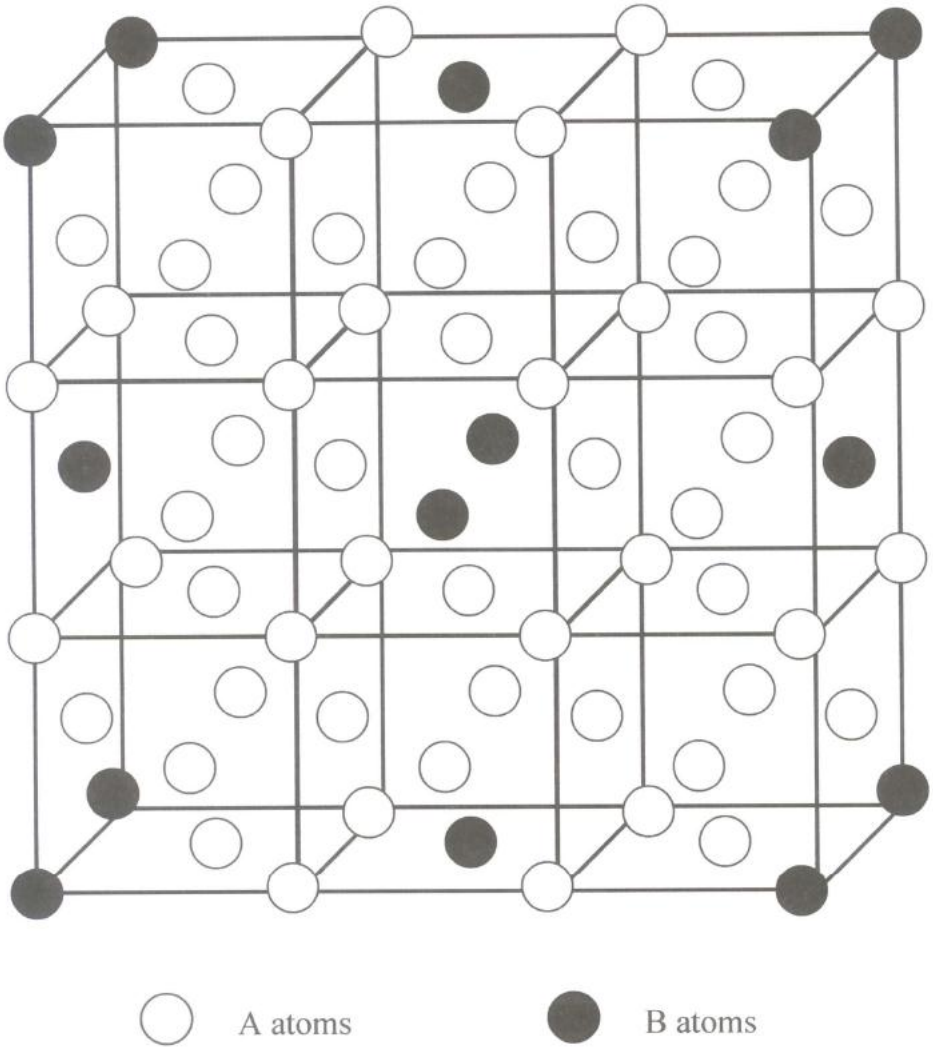

Figure 2.5: The (fct) A_8B superlattice structure (after Quist *et al.* [22]).

Ardell [2] tabulated the results obtained from the experimental procedure of Pietrokowsky [23] and Schryvers and Amelinckx [24], as shown in table 2.3.

Table 2.3 shows the different A_8B alloys with their respective transformation temperatures of some already obtained. $\mathbf{a}_m$ is the lattice constant of the disordered matrix for all the phases except Pt_8X, for which this symbol is used to represent $\mathbf{c}_0$. The dimensions of unit cells are $\mathbf{c}_0 = \mathbf{a}$, $\mathbf{a}_0 = 3\mathbf{a}/\sqrt{2}$ and $\mathbf{a}_0' = 3\mathbf{a}$. Out of all the A_8B phases Pt_8Ti is so far the only phase for which $\mathbf{a}_0'/3\mathbf{c}_0 > 1$ and that the lattice constant of the disordered Pt 11.1 % at. Ti solid solution is not known. It is evident that the T_c of the Pt_8X (except T_c = 810 ° for Pt_8V which was recently discovered [21]) even not known is much higher than in Ni and Pd-base alloys and clearly exceeding 1000 °C for Pt_8Zr.

Table 2 3: Lattice constants and critical ordering temperatures for A_8B phases [2].

	% X	$\mathbf{a}_m$ (nm)	$\mathbf{a}_o$ (nm)	$\mathbf{a}_o'/3\mathbf{a}_m$	T_c (°C)
Ni_8Mo	8.0	---	---	---	242
	10.0	---	---	---	282
	11.1	---	---	---	282
	13.0	---	---	---	197
Ni_8Nb	10.3	---	---	---	535
	11.1	0.3593	0.7612	0.9987	540
Ni_8Ta	11.1	0.3589	0.7604	0.9988	570
Ni_8V	11.1	---	---	---	405
Pd_8Mo	10.0	0.3889	0.8238	0.9986	430 (max)
	18.0	---	---	---	600 (max)
Pd_8V	15.0	---	---	---	400 (max)
Pd_8W	10.0	0.3888	0.8245	0.9997	735
Pt_8Ti	11.1	0.3897	0.8312	1.0055	---
Pt_8V	11.1	0.3900	0.8200	0.9910	---
Pt_8Zr	11.1	0.4207	0.8386	0.9817	---

In 1968 *Krautwasser et al.* [25] mentioned the existence of the Pt_8Zr phase over the temperature range 750 to 1000 ˚C in an alloy of Pt 11 at. % Zr. The Pt_8Zr phase was also

observed by Meschter and Worrell for the composition Pt 10 at. % Zr alloy, over the temperature range 827 to 1027 °C [26], in an investigation of Pt-Zr alloys containing between 2 and 22 atomic per cent Zr over that temperature range (827 to 1027 °C) [26].

Meschter and Worrel [26] combined results obtained by previous researchers [9,25] with X-ray analyses of Pt-Zr alloy-oxide (probably < 0.1 at. %) samples containing 2, 5, 10, 15, 17, 20 and 22 at. % Zr. Figure 2.6 shows the phase relationships of the alloys. It illustrates the occurrence of the single and two phase configuration of the platinum-zirconium alloys according to atomic per cent composition of zirconium. Krautwasser *et al*. [25] studied the 11.1 at. % Zr and found that a single phase occurs at about 1000 K and 1300 K. Meschter and Worrel [26] also found that a single phase for the 10 at. % Zr occurs approximately 1100 K and 1300 K. This is consistent with the prediction that the Pt_8Zr phase exist along that temperature range.

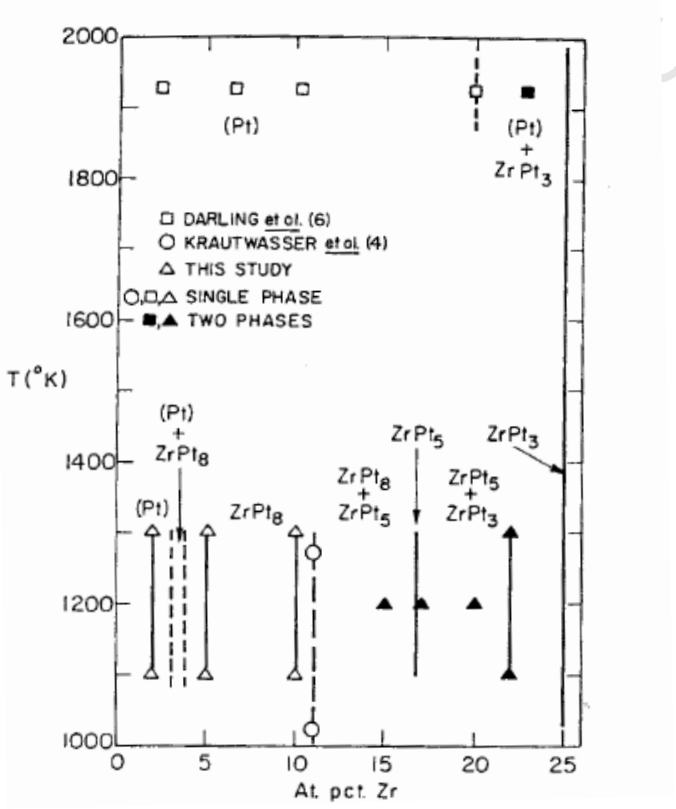

Figure 2.6: Shows the Pt-Zr phases from 0 to 25 at. % Zr (after Meschter and Worrell [26]).

2.4 The Platinum-Zirconium Equilibrium Phase Diagram

The platinum-zirconium phase diagram was first studied by Kendall *et al*. [27] for Zr-rich alloys up to 50 at. % Pt. The phase diagram for the platinum rich alloys up to Pt 25 at.% Zr was published by Fairbank *et al.* [28], but the equiatomic region around Pt 50 at.% Zr has never been fully investigated. Fairbank *et al.* [28] confirmed the existence of an $L1_2$-like phase for the following alloys: Pt_3Zr, Pt_4Zr and Pt_5Zr (which appears to be centred on the composition Pt_4Zr). Raman and Schubert [29] reported compounds at the compositions ZrPt, Zr_4Pt_5 and Zr_2Pt_3. Stalick and Waterstrat [30] experimentally investigated the phase relationships and crystal structures of ZrPt, Zr_9Pt_{11}, Zr_3Pt_4, Zr_7Pt_{10} and $Zr_{47}Pt_{53}$ compositions using X-ray diffraction, high-temperature neutron diffraction and optical microscopy. Below are some of the results obtained.

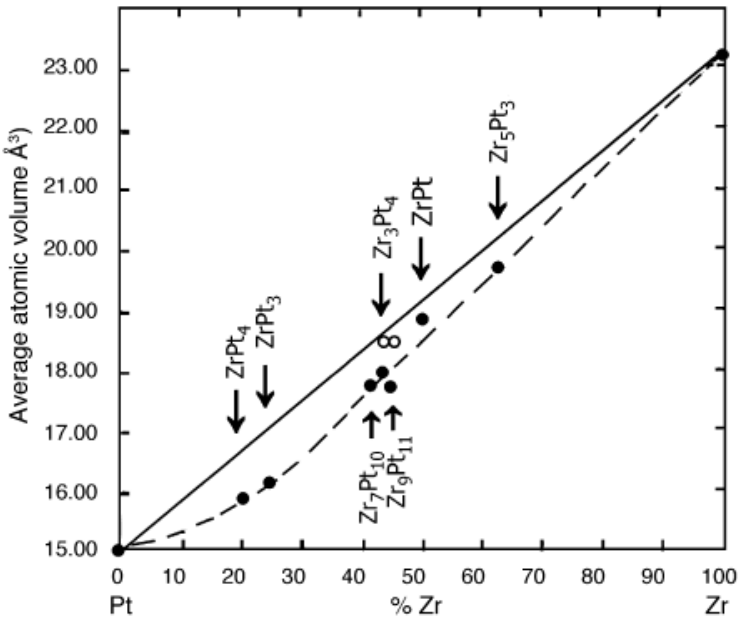

Figure 2.7: Average atomic volumes vs. composition for Pt-Zr alloys. The open circles represent the tetragonal phase and the closed circles represent the triclinic or rhombohedral phase (after Stalick and Waterstrat [30]).

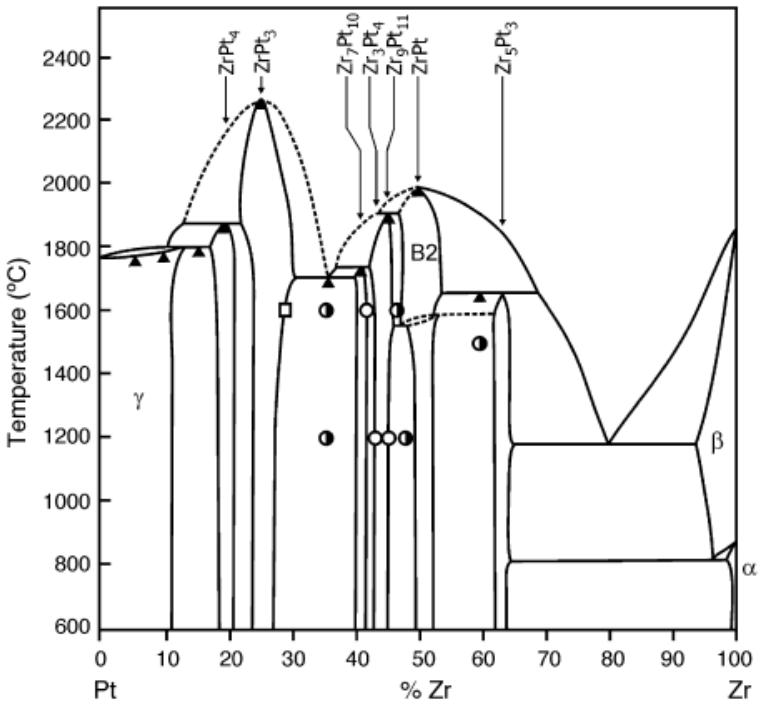

Figure 2.8: Phase diagram of the Pt-Zr system. The triangles indicate the onset of melting on heating; half-filled circles indicate a two-phase alloy; open circles indicate a single-phase alloy (after Stalick and Waterstrat [30]).

Figure 2.8 shows combined results by Kendall *et al*. [27] and Fairbank *et al*. [28] with the results obtained by Stalick and Waterstrat [30]. Stalick and Waterstrat [30] have constructed a complete phase diagram for the Pt-Zr system, and it also shows solidus data that previous researchers did not include. Figure 2.9 below also shows a complete equilibrium phase diagram of the platinum-zirconium system with a peritectic transformation of Pt_4Zr at 1880 ± 10 °C and a congruent melting of Pt_3Zr at 2250 °C [30].

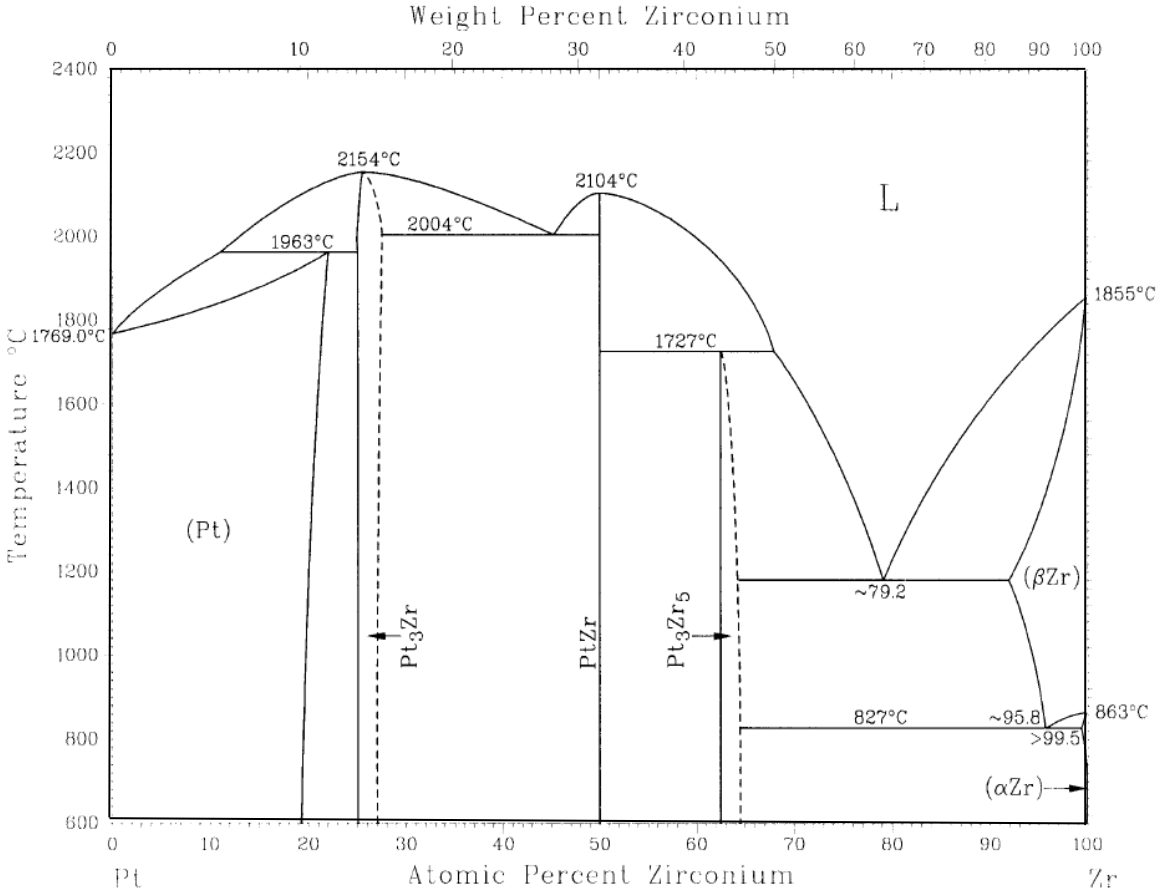

Figure 2.9: The platinum-zirconium equilibrium phase diagram (after Stalick and Waterstrat [30]).

2.5 The Platinum-Vanadium System

The platinum-vanadium system was first investigated by Waterstrat [31], who studied the entire composition range above 700 °C using metallography, X-ray diffraction and electron microscopy. There are at least four equilibrium intermediate phases that are stable [31], as shown in figure 2.10.

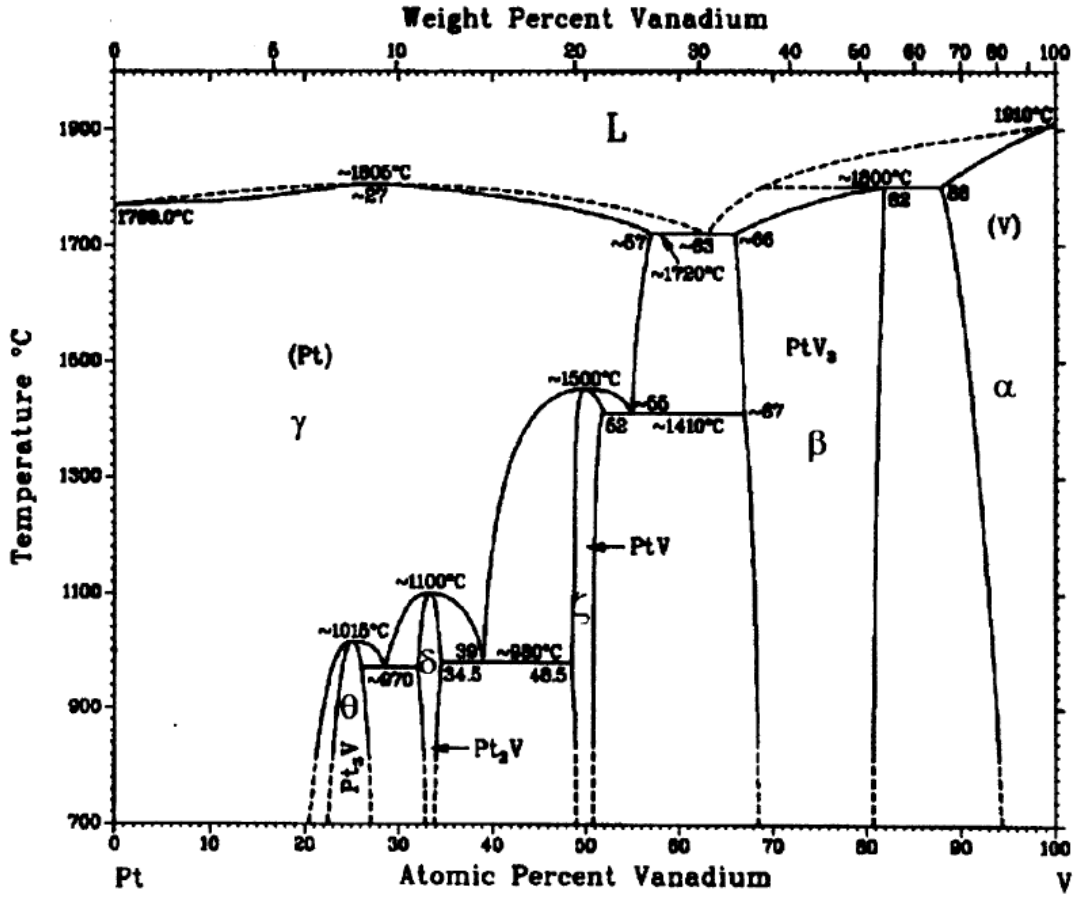

Figure 2.10: The platinum-vanadium equilibrium phase diagram (after Waterstrat [31]).

The phases observed by Waterstrat are: ɣ'(cubic, Cu_3Au type); ɵ(tetragonal, $TiAl_3$ type); δ(orthorhombic, $MoPt_2$ type); ζ(orthorhombic, AuCd type); and β(cubic, Cr_3Si type). The ɣ phase forms a congruent melting maximum at about 1805 ˚C. A eutectic and a peritectic reaction occurs at about 1720 ˚C and 1800 ˚C respectively. Vanadium is soluble in the fcc platinum solid solution at 1720 ˚C up to about 57 at % V but platinum is soluble in V at 1800 °C only to about 12 at. % Pt [31].

In the presence of excess vacancies, Pt 11 at. % V undergoes an ordering transformation forming Pt_8V [24], with a transformation temperature of 810 ± 10 ˚C, according to Nxumalo and Lang [21]. The ordering transformation process requires diffusion which is favoured by an enhanced vacancy concentration. In the above mentioned work, vacancies are introduced into the alloy by quenching or by deformation allowing vacancies to enhance the phase transformations by allowing atoms to freely occupy preferred sites. These phase transformations are accordingly sensitive to vacancy concentration.

2.6 The Effect of Hydrogen on Phase Transformations

Hydrogen has been found by Qazi *et al.* [4] to affect the alpha-beta phase transformation in Ti-6Al-4V alloy: an increase in hydrogen concentration from 0 to 30 % in Ti-6Al-4V decreases the beta-transus temperature from 1005 ˚C to 815 ˚C [4].

Narita *et al.* [5] reported that hydrogen stabilizes the austenite in Fe-Cr-Ni stainless steels. Hydrogen also promotes the transformation of the fcc ɣ phase to the fcc ɣ* phase (which has a larger lattice parameter than ɣ phase) and hcp Ɛ (martensite) phases in stainless steels. Below is a pseudo-binary phase diagram for the stainless steel-hydrogen system, which shows a miscibility gap between the ɣ and ɣ* phases at a critical hydrogen concentration range. When the composition $ɣ_e$ is exceeded, the fcc phase of composition $ɣ_e$* is able to form.

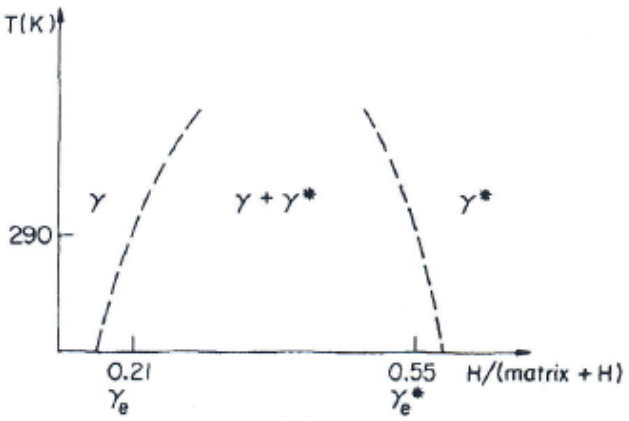

Figure 2.11: Proposed pseudo-binary phase diagram for the stainless steel-hydrogen system (after Narita *et al*. [5]).

Avdyukhina *et al.* [6] investigated hygrogen-induced phase transformations in a Pd-8.3 at. % Y alloy, reporting that during hydrogenation, there was a substantial increase in the diffusion coefficient of yttrium atoms. X-ray results showed that when the alloy was subjected to saturation with hydrogen and relaxation for 840 hours at room temperature, decomposition into two co-existing phases (α solid solution of Pd-Y-H and an ordered Pd_7Y-H phase) occurs.

Sakamoto *et al.* [8] studied the hydrogen-induced suppression of ordering to Pd_7M (M = Sm, Gd, Li) (Pt_7Cu-type superlattice), reporting that suppression of short range order occurs at hydrogen pressures of > 20 bar. This suppression effect may be due to the retardation of nucleation and growth of the ordered domains during cooling, caused by the weakening of the Pd-M bond by the dissolved hydrogen.

2.7 Literature Review Summary and Hypotheses

Pt 11 at. Zr has been predicted to undergo an ordering transformation, thereby forming the Pt_8Zr phase with the transformation temperature (T_c) between the temperature range 827 and 1027 °C [26]. The formation of ordered domains as a resultant of ordering increases the hardness of Pt 11 at. % X (X= vanadium and chromium) as reported by Nxumalo *et al*. [3]. Hydrogen has been found to affect the kinetics of phase transformations in some alloys [4,5,6,8]. The experimental procedure outlines the experiments conducted to obtain the Pt_8Zr ordered phase, as well as the techniques used to examine this ordered phase; the effect of hydrogen on the ordering transformations of the Pt 11 at. % V and the techniques used to investigate this effect.

Therefore, it is hypothesized that:

- Pt_8Zr phase will be formed with a T_c between 827 and 1027 °C.
- The hardness of the Pt 11 at. % Zr will increase with the formation of the Pt_8Zr phase.
- Hydrogen will enhance the ordering kinetics of the Pt 11 at. % V alloy.

3. EXPERIMENTAL PROCEDURES

3.1 Alloy Preparation

Platinum-zirconium and platinum-vanadium buttons were prepared in the same manner. The respective masses were first weighed out using a *Sartorius Research R200D* electronic balance to make up the Pt 11 at. % Zr and the Pt 11 at. % V compositions. The elements were then melted together at Mintek using a button-arc furnace under an argon atmosphere. Pure titanium button was melted first, as titanium acts as an oxygen scavenger to prevent oxidation during melting of samples. Tungsten electrode is utilised to strike an arc with the material to be melted utilising a welding transformer as a power source. The platinum-vanadium button was melted three times, turning the sample over during melting to ensure a homogenous alloy button. However, the platinum-zirconium button was melted more than three times as it would form cracks due to the brittleness of the zirconium. Hence no homogenisation heat treatment was necessary for the platinum-zirconium button.

3.1.1 Platinum-Zirconium

3.1.1.1 Isochronal heat treatments

Scanning electron microscopy was used to confirm the composition and the homogeneity of the button. A spot (10 points across the button) analysis was performed across the button and confirmed homogeneity after solidification. EDS (see section 3.1.2.1) showed that the button was approximately 99 % pure and 99 % homogeneous. The Pt 11 at. % Zr button was sliced into thin 3mm thick specimens using a *Buehler* Isomet. The specimens were then subjected to isochronal heat treatments between 800°C and 1200°C for a duration of 3 hours using a laboratory furnace. A *Foseco Isomol 100* anti-oxidant was used to coat the samples to prevent oxidation. All the heat treatments were terminated by water quenching.

3.1.1.2 Light microscopy

The sliced specimens were used for light microscopy. A *Labopress-3* hot mounting machine was used to mount the specimens in resin. SiC paper of 800 and 1200 grit was used to grind

the specimens using water as a lubricant. The specimens were then polished using a 3 µm, 1 µm and finally a 0.25 µm diamond paste to obtain a mirror finish. Grains were then observed on the surface without using an etchant. Light microscope images were obtained using a *Reichert MeF3A* light microscope in Normarski mode, and a *Leica DFC320* digital camera.

3.1.2 Platinum-Vanadium

3.1.2.1 Button deformation and homogenisation heat treatment

The Pt 11 at. % V button was first deformed to reduce the thickness by 50% using a *Dinkel* laboratory rolling mill. This deformation was done in order to aid homogenisation. A homogenisation heat treatment was carried out at 1000˚C in vacuum for 23 hours. A homogenisation heat treatment involves the heating of the alloy at 80% the melting temperature in order to enable atoms to move around down any concentration gradient until equilibrium is reached.

3.1.2.2 Scanning electron microscope

A *Nova Nano* SEM (scanning electron microscope) *230* with EDS (Energy Dispersive Spectrometer) was used to confirm the homogenisation of the specimen. EDS analysis measures the energy and intensity distribution of X-ray signals generated by the electron beam on the specimen. A 20 mm^2 X-Max detector was used for this X-ray analysis.

Table 2.4: Atomic levels for platinum, vanadium and zirconium [36].

Element	M_α (eV)	L_α (eV)	K_α (eV)
Pt	2.0485	9.4424	68.820
V	-	0.5113	4.9498
Zr	-	2.0424	15.7473

A beam of 20 keV was used to excite the x-ray lines for the platinum and vanadium analysis. Electrons at the M and L atomic levels were excited for the platinum but L and K atomic

levels for the vanadium. To excite electrons at the K atomic level for the zirconium, a higher voltage beam of 30 keV was used.

An *INCA* software was used to identify the elements. A spot/line (10 points) compositional analysis was performed across the button and an average was taken. The average obtained was approximately Pt 11 at. % X (X = V and Zr) composition. The SEM/EDS analysis is not accurate below 1% therefore, only the major elements such as Pt, V and Zr are reported. If minor elements less than 1 wt % were present are therefore not reported.

3.1.2.3 Isochronal heat treatments

A further 90% reduction of the specimen thickness was obtained by rolling using the *Dinkel* laboratory rolling mill, to produce a sheet that was approximately 400 µm thick. The sheet was punched into thin discs of 3 mm in diameter which were placed in a small crucible for heat treatments. A controlled atmosphere tube furnace was used for the heat treatments. The heat treatments were performed in two different media, one in 15% hydrogen (85% argon, by volume) and the other in vacuum. Isochronal heat treatments were carried out at temperatures between 400˚C and 900˚C for a period of 3 hours and were furnace cooled.

3.1.2.4 Light microscopy

After heat treatments a *Labopress-3* hot mounting machine was used to mount the samples in resin. 1200 grit SiC paper was used to grind the specimens using water as a lubricant. The specimens were then polished using a 3 µm, 1 µm and finally a 0.25 µm diamond paste to obtain a mirror finish. A mixture of 25 g NaCl, 25 ml HCl and 65 ml distilled water was used as the etchant. An alternating current was used at a voltage of 10 V with an etching time from 30 to 60 s. A stainless steel clamp was used as the anode and a graphite rod as the cathode. Light microscope images were obtained using a *Reichert MeF3A* light microscope in bright light mode and a *Leica DFC320* digital camera.

3.2 Hardness Measurements

Specimens used for light microscopy was also used to obtain hardness measurements. The specimens were reground and repolished as described above to obtain a mirror finish. A *Zwick* digital microhardness tester using a standard Vickers diamond indenter with a 300 gf

load was used for the platinum-vanadium samples and a 500 gf load was used for the platinum-zirconium specimens.

3.2.1 Indentation Depth and Sample Thickness

Elastoplastic deformation of materials around the indenter can make it difficult to determine the true contact depth in the loaded state. The contact depth can be determined by an equation derived from the Oliver and Pharr method [38].

$H_d = \varepsilon (P_{max}/ S)$ **Equation 3.1**

$HV = [P_{max} / 26.43 (h_c^v)^2]$ **Equation 3.2**

Where $H_d = h_c^v$ = contact depth

P_{max} = indentation force

HV = hardness value

S = initial unloading stiffness

ε = geometrical constant

The thickness of the sample under test should be at least ten times the permanent depth of indentation for the diamond cone indenter [39].

3.3 Transmission Electron Microscopy

Owing to the brittleness of the platinum-zirconium alloy, a spark erosion unit was used to extract 3 mm discs from the thin specimen slices. The discs were ground using a 1200 grit SiC paper, from about 3 mm to a 100 µm thickness using water as a lubricant. The platinum-vanadium specimens were ground down from about 400 µm to about 100 µm using 1200 grit SiC fine grinding paper with water as a lubricant. A *Gatan* dimpler was used to reduce the thickness of the centre of the discs from 100 µm to 30 µm for both alloys. This was followed by milling to perforation using a *Gatan Precision Ion Polishing System* (PIPS). Argon gas was used to mill the discs to perforation, operating at a voltage of 5 kV. The ion guns were set at angles between 3° and 6°. Perforation occurred after a minimum of 10 hours.

An FEI F20 electron microscope was used at a voltage of 200 kV to carry out transmission electron microscopy (TEM). The electron beam was fully spread to achieve parallel illumination for obtaining electron diffraction patterns and imaging. A 10 µm and 40 µm objective aperture was used to select areas for the electron diffraction pattern. A duration

of between 0.5 to 3 seconds was used as the exposure time. The dark field images were obtained using a 30 µm diffraction aperture. The exposure time used for the dark field images varied between 1 to 5 seconds.

3.3.1 Preparation of Thin Foils

Three 100 µm discs were prepared for each measurement. On average 2 out of three samples were successfully perforated using the *Gatan Precision Ion Polishing System* (PIPS).

Area of disc = $\pi r^2 = \pi (1.5)^2 = 7.07$ mm^2

Area of thin surface ≈ 20 % of area of disc ≈ 1.41 mm^2

Area of perforation ≈ 10 % of area of disc ≈ 0.71 mm^2

Therefore, the area analysed using TEM was approximately 0.71 mm^2.

The desired area used to analyse was approximately 0.71 mm^2, but this was not the case for all samples. An area less than 0.71 mm^2 was used to analyse some samples, however this did not affect the results obtained. The area was still big enough to successfully obtain the diffraction patterns and dark field images of the alloys.

3.4 Differential Scanning Calorimetry (DSC)

DSC is a thermal analysis technique that measures the temperature at which any phase change occurs. A *Netzsch STA 409* thermal analyser fitted with an S-type thermocouple, operating at a maximum temperature of 1500 °C was used. The samples weighed approximately 20 mg and an alumina (Al_2O_3) crucible was used. The temperature profiles for the Pt 11 at. % Zr alloy and Pt 11 at. % V were the following respectively: room temperature – 1200 °C (which was selected as it is above the predicted transformation temperature), at rate of 15 min/°C, followed by an isothermal holding time of 10 minutes, and finally a cool down from 1200 °C to room temperature; room temperature – 1000 °C, isothermally held for 10 minutes, cooled to 700 °C, isothermally held for 12 hours, and finally cooled from 700 °C to room temperature.

During the heating and cooling sequences, Argon gas was set to flow through the balance of the DSC holder at a constant rate of 50 ml/ min. The curves of heat flow vs. temperature were plotted using the *Netzsch Proteus* analysis programme. The maximum data acquisition rate was 600 data points/minute.

4. RESULTS

This chapter shows the results of two investigations: determining the ordering characteristics and transformation temperature of Pt 11 at. % Zr; and evaluating the effect of hydrogen on ordering in the Pt 11 at. % V alloy. In both cases, transmission electron microscopy with electron diffraction was used to characterise the ordered and disordered states. The effect of temperature was evaluated using heat treatments; light microscopy and microhardness testing were also carried out.

4.1 The Platinum-Zirconium System

Transmission electron diffraction results, which shows the temperature range in which the Pt_8Zr structure exists, are presented first followed by hardness measurements which show the effect of ordering on hardness. Light microscopy is presented to show the effect of these heat treatments on microstructure. Finally, DSC results are presented to show phase transformation events as a function of temperature.

4.1.1 Electron Diffraction Patterns

Zone axis electron diffraction patterns are shown for each heat treatment temperatures. Four zone axes, namely $[001]_{fcc}$, $[011]_{fcc}$, $[112]_{fcc}$, and $[013]_{fcc}$, are shown below. Figure 4.1.1a shows electron diffraction patterns in a simulation of the well-documented Pt_8V superlaticce containing fundamental fcc reflections and superlattice reflections. It is expected that all A_8B superlattices will exhibit diffraction patterns that are consistent with this simulation. The geometry of the electron diffraction patterns were simulated using the JSV1.08 structure viewer software program developed by C.S. Weber (http://www.jcrystal.com/steffenweber/JAVA/JSV/jsv.html) [40].

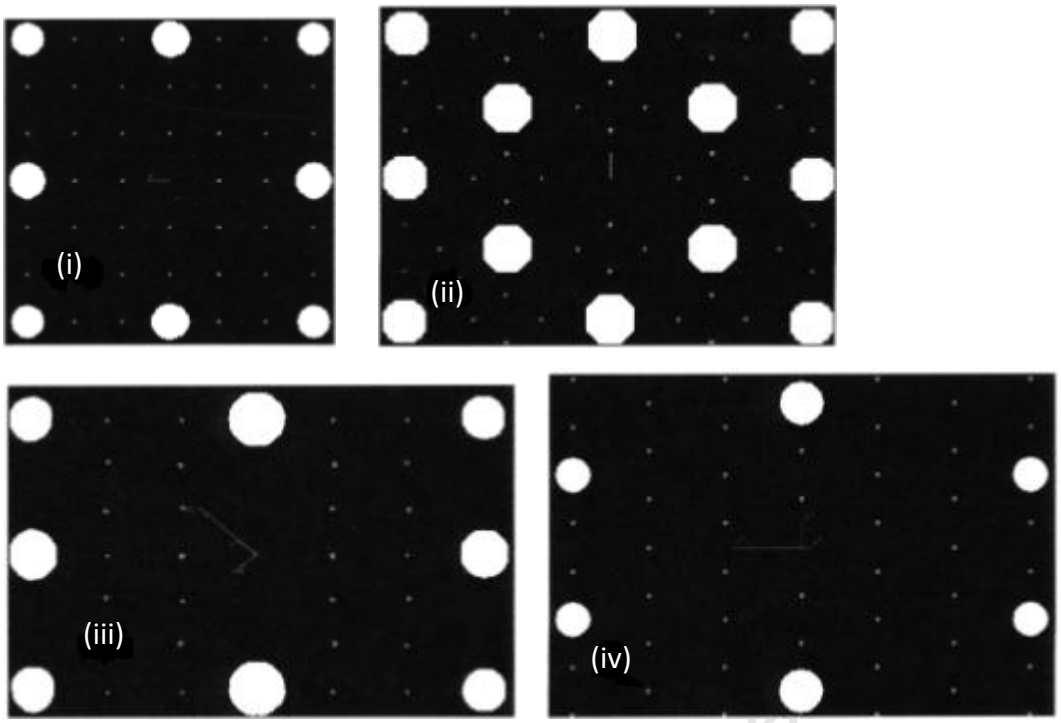

Figure 4.1.1a: Simulated zone axis electron diffraction patterns for an A_8B alloy showing (i) [001]fcc, (ii) [011]fcc, (iii) [112]fcc, (iv) [013]fcc zone axes. The large spots are the fundamental fcc reflections; the small spots are the A_8B superlattice reflections.

4.1.1.1 The effect of heat treatment temperature on Pt 11 at. % Zr alloys

Isochronal heat treatments of cast platinum-zirconium were performed at temperatures up to 1200°C for a duration of 3 hours. The as-cast (initial condition) specimen, and specimens heat treated up to 1070°C, exhibited electron diffraction patterns containing additional reflections as shown in Figures 4.1.1b to 4.1.1f. The specimens heat treated at 1090°C and above showed only fundamental fcc reflections as shown in Figure 4.1.1g. The specimens heat treated at 1000 °C, showed electron diffraction patterns identical to specimens at 1090 °C and are not included.

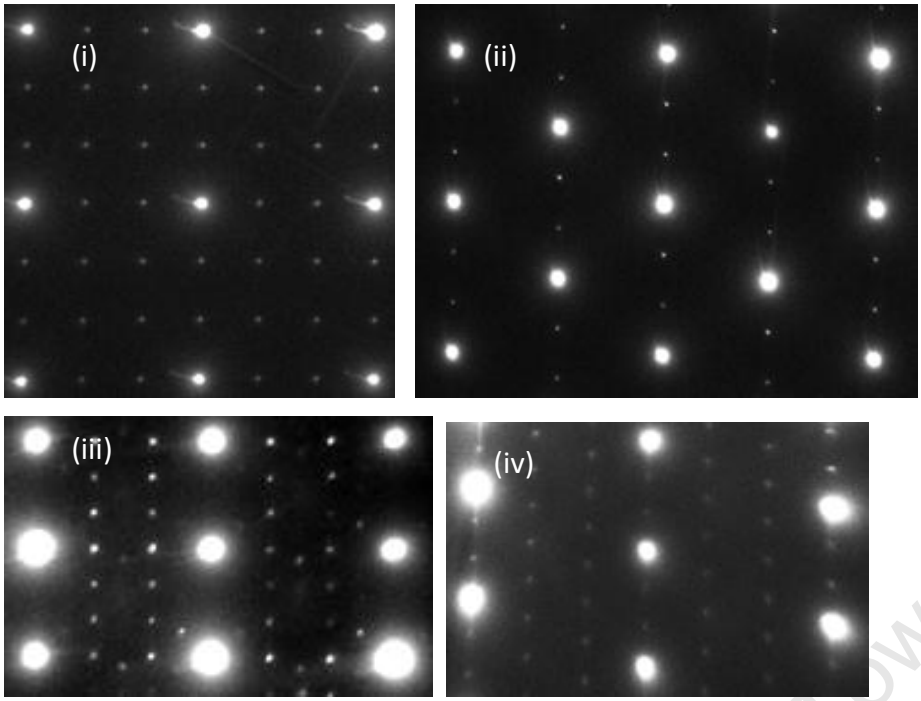

Figure 4.1.1b: Zone axis electron diffraction patterns for as-cast specimen of platinum-zirconium showing (i) [00-1]fcc, (ii) [0-11]fcc, (iii) [-1-12]fcc and (iv) [0-13]fcc zone axes.

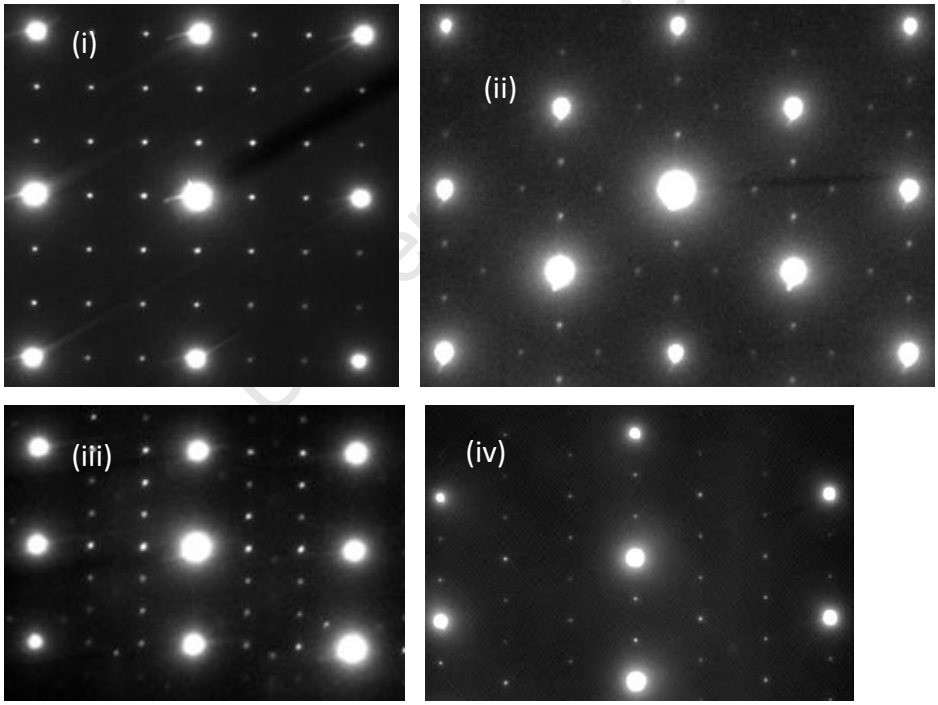

Figure 4.1.1c: Zone axis electron diffraction patterns for platinum-zirconium after heat treatment at 800 °C for 3 hours showing (i) [00-1]fcc, (ii) [0-11]fcc, (iii) [-1-12]fcc and (iv) [0-13]fcc zone axes.

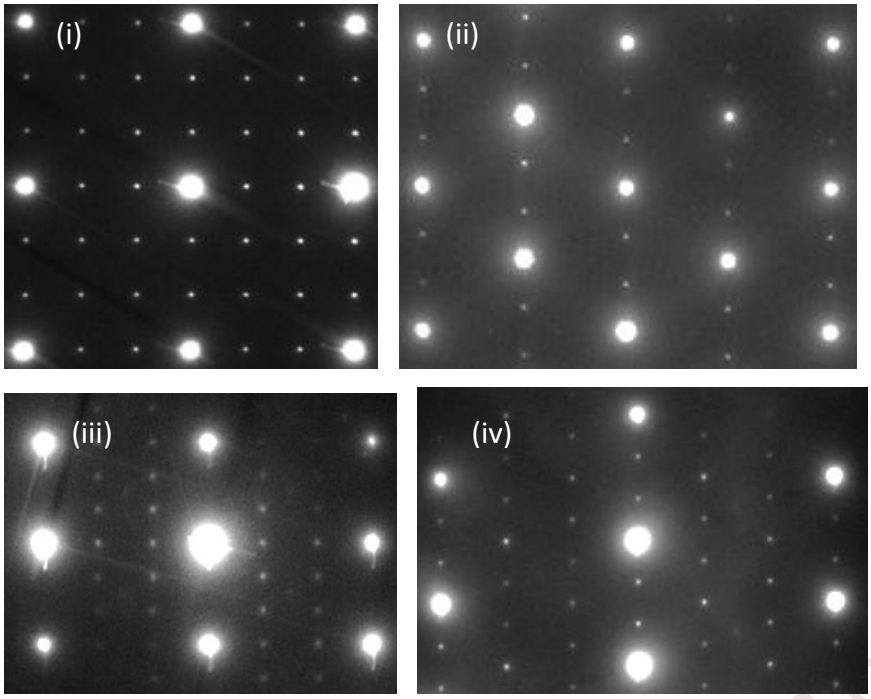

Figure 4.1.1d: Zone axis electron diffraction patterns for platinum-zirconium after heat treatment at 1000°C for 3 hours showing (i) [00-1]fcc, (ii) [0-11]fcc, (iii) [-1-12]fcc and (iv) [0-13]fcc zone axes.

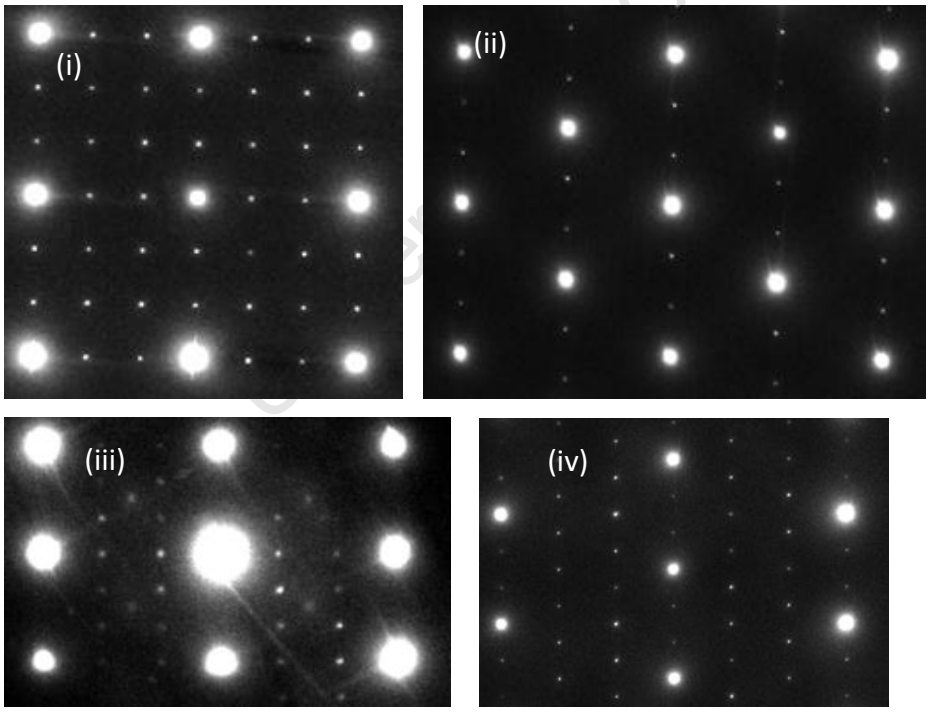

Figure 4.1.1e: Zone axis electron diffraction patterns for platinum-zirconium after heat treatment at 1050°C for 3 hours showing (i) [00-1]fcc, (ii) [0-11]fcc, (iii) [-1-12]fcc and (iv) [0-13]fcc zone axes.

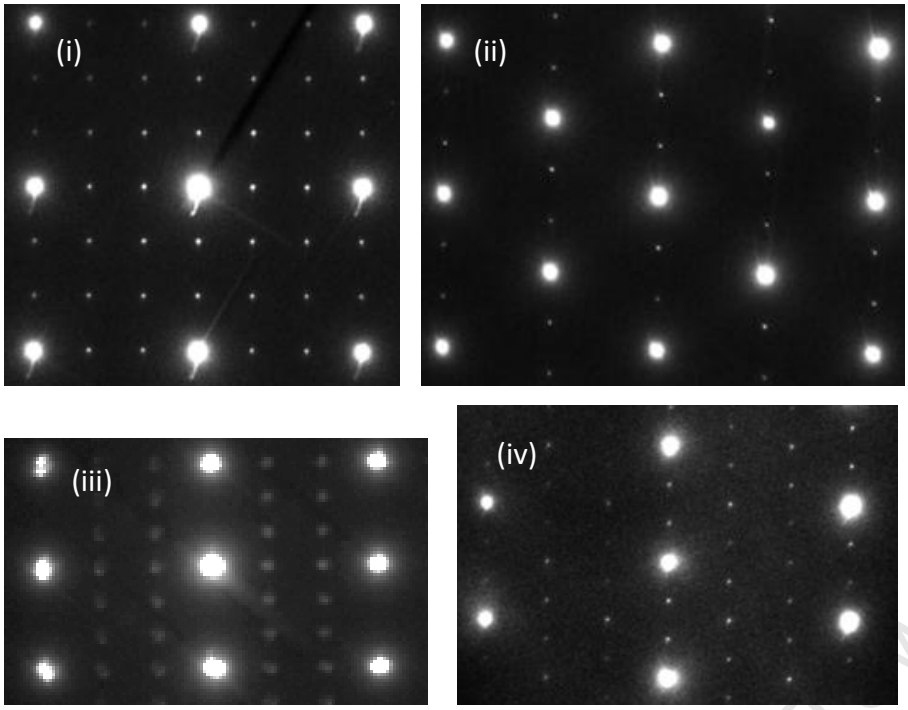

Figure 4.1.1f: Zone axis electron diffraction patterns for platinum-zirconium after heat treatment at 1070°C for 3 hours showing (i) [00-1]fcc, (ii) [0-11]fcc, (iii) [-1-12]fcc and (iv) [0-13]fcc zone axes.

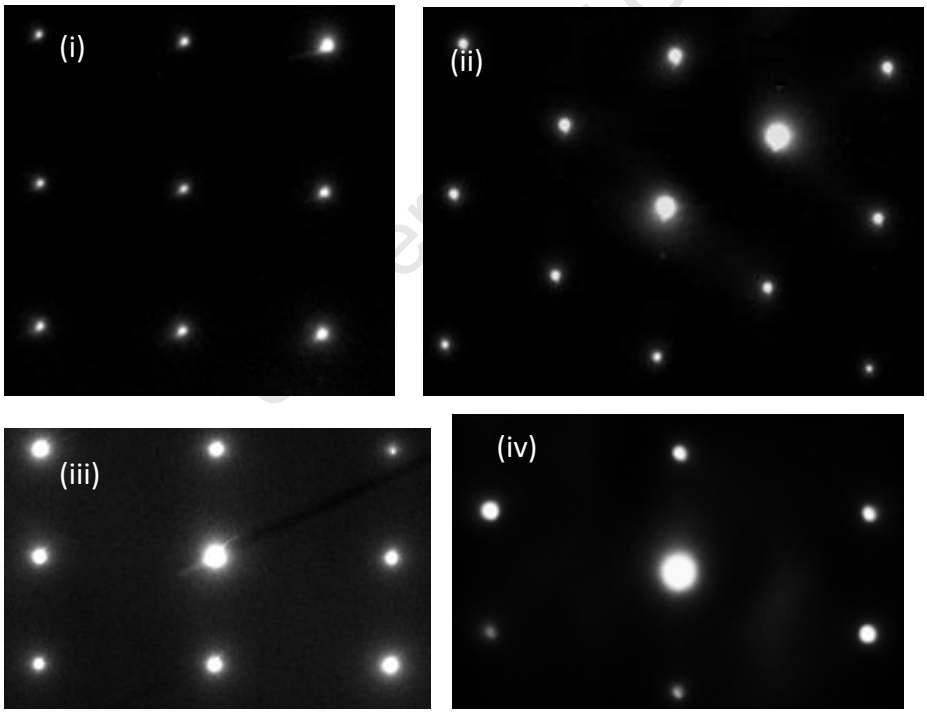

Figure 4.1.1g: Zone axis electron diffraction patterns for platinum-zirconium after heat treatment at 1090°C for 3 hours showing (i) [00-1]fcc, (ii) [0-11]fcc, (iii) [-1-12]fcc and (iv) [0-13]fcc zone axes.

4.1.2 TEM Dark Field Imaging

The electron diffraction patterns shown in section 4.1.1 which exhibited additional reflections are consistent with the formation of Pt_8Zr as shown by comparison with figure 4.1.1a. Dark field images were acquired from the platinum-zirconium TEM specimens, using the additional reflection arrowed in figure 4.2.1a to figure 4.2.1f.

The ordered domains can be clearly defined using the digital micrograph programme in the TEM. Figure 4.1.2 below shows how one ordered domain is represented and clearly defined. The ordered domains are shown in bright contrast in all the dark field images, however some areas (refer to A) may appear to be much brighter than others which suggest a larger domain, but this is more likely to represent a cluster of several much smaller domains.

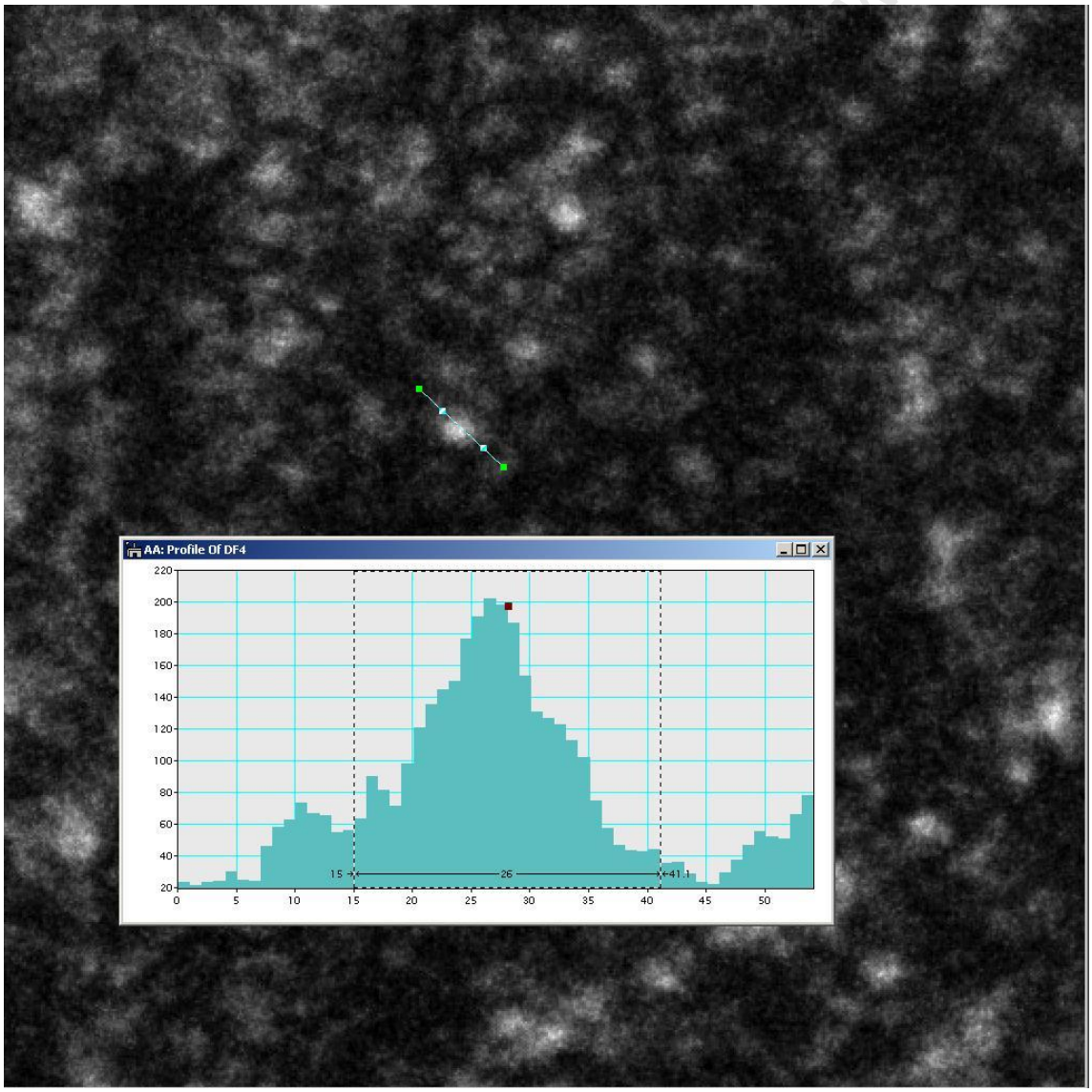

Figure 4.1.2: Shows an ordered domain defined using an intensity profile.

4.1.2.1 The effect of heat treatment temperature on domain size

The as-cast initial condition for Pt 11 at. % Zr alloy and alloys heat treated up to a temperature of 1070 °C, showed the presence of ordered domains of Pt_8Zr. The ordered domains are in bright contrast as shown in figure 4.1.2a to 4.1.2e below. The ordered domains are around 5 to 10 nm in diameter in all the dark field images, for the as-cast specimen and all the specimens heat treated between 800 °C and 1070 °C.

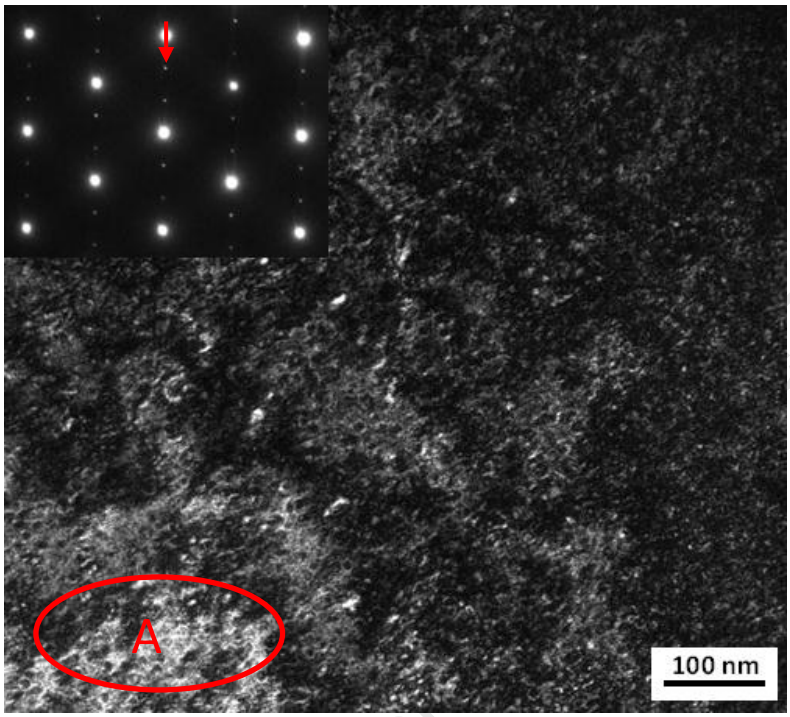

Figure 4.1.2a: Dark field image, obtained using the arrowed reflection, for as-cast platinum 11 at. % zirconium, showing ordered precipitates in bright contrast.

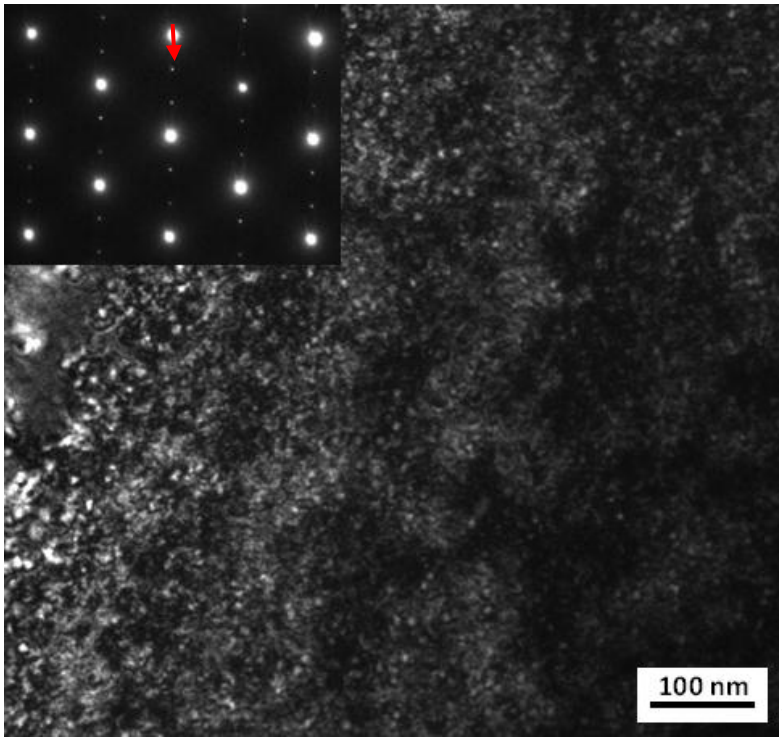

Figure 4.1.2b: Dark field image, obtained using the arrowed reflection, of 800 °C/3 hour heat treated platinum 11 at. % zirconium, showing ordered precipitates in bright contrast.

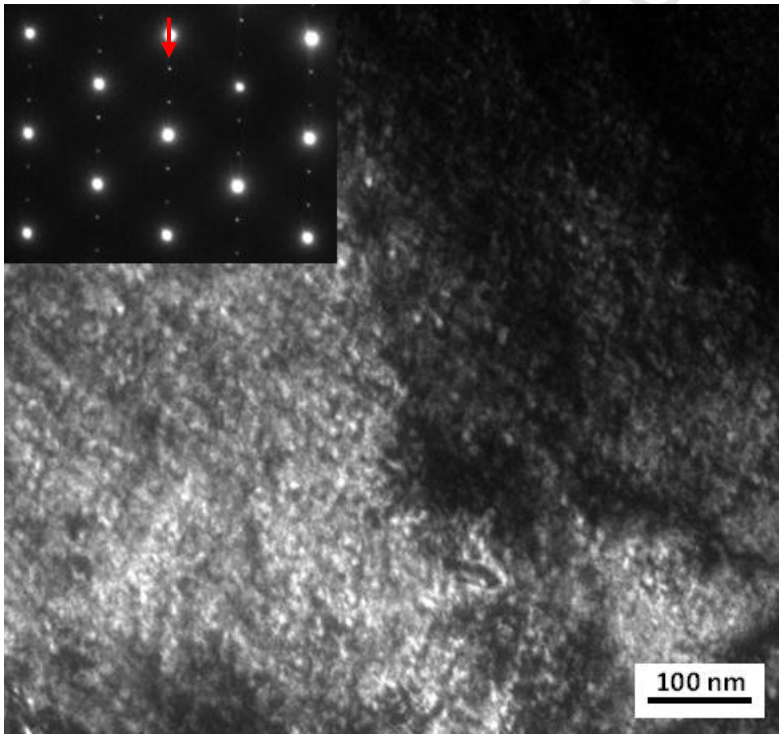

Figure 4.1.2c: Dark field image, obtained using the arrowed reflection, of 1000 °C/3 hour heat treated platinum 11 at. % zirconium, showing ordered precipitates in bright contrast.

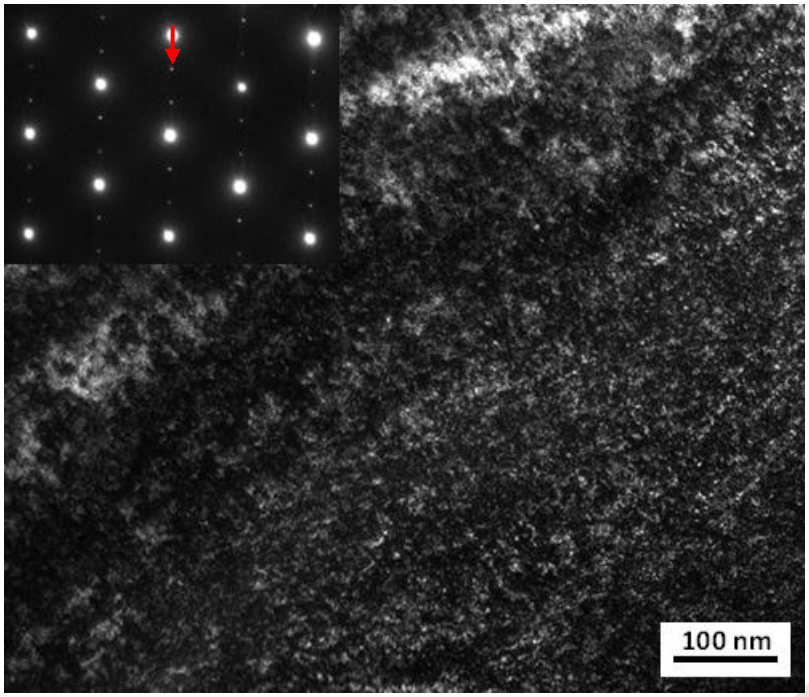

Figure 4.1.2d: Dark field image, obtained using the arrowed reflection, of 1050 °C/3 hour heat treated platinum 11 at. % zirconium, showing ordered precipitates in bright contrast.

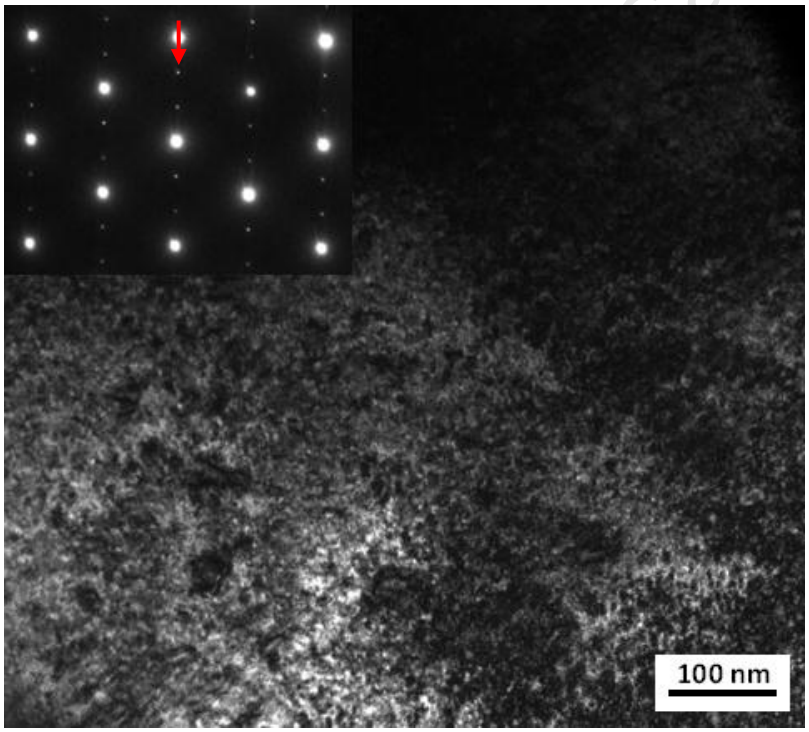

Figure 4.1.2e: Dark field image, obtained using the arrowed reflection, of 1070 °C/3 hour heat treated platinum 11 at. % zirconium, showing ordered precipitates in bright contrast.

4.1.2.2 The effect of heat treatment time on domain size

A Pt 11 at. % Zr specimen was subjected to 600 hours heat treatment at a temperature of 1000 °C. TEM was used to obtain the dark field image, using the arrowed reflection, shown in Figure 4.1.2f below.

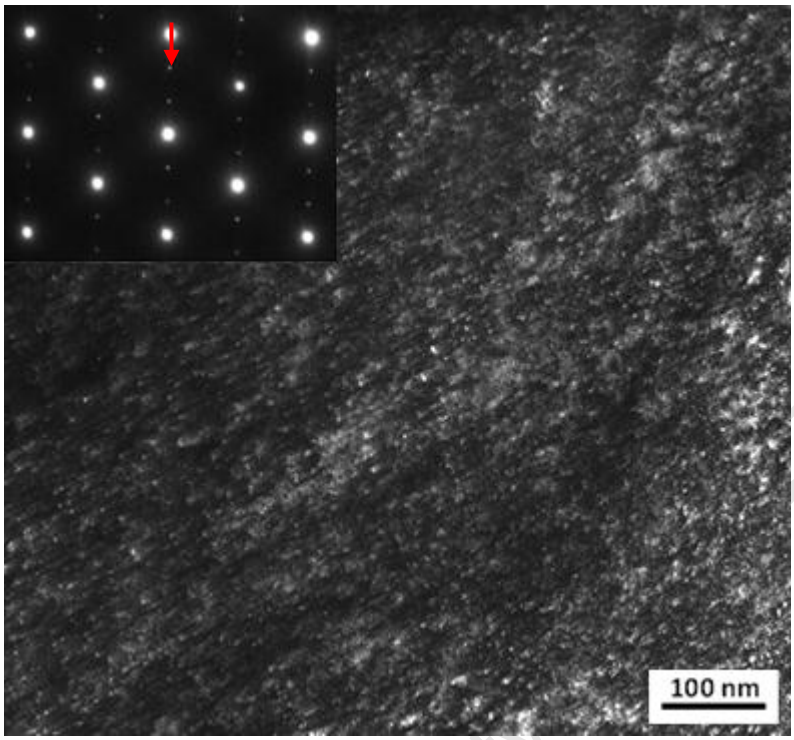

Figure 4.1.2f: Dark field image, obtained using the arrowed reflection, of 1000 °C/600 hour heat treated platinum 11 at. % zirconium, showing ordered precipitates in bright contrast.

Compared with figure 4.1.2c, which shows a dark field image of a specimen heat treated at 1000 °C for 3 hours, figure 4.1.2f shows no significant growth of domains. The ordered domains appear to remain constant in size with time, even at elevated temperatures.

4.1.3 Hardness Measurements

For every heat treatment temperature, two heat treatments were conducted for the same temperature and time. Ten hardness measurements were taken for each heat treatment temperature. The thickness of the sample was approximately 400 µm. Referring to section 3.2.1, the thickness of the test sample should be at least 10 times the permanent depth of indentation for the diamond cone indenter. Equation 3.2 can be used to work out the contact/permanent depth.

$HV = [P_{max} / 26.43 (h_c^v)^2]$

P_{max} = 500 gf = 4903.33 mN

Hardness = 430 HV and 100 HV (using the highest and lowest values).

H_c^v = 0.66 µm and 13.62 µm

The final thickness after polishing was approximately 210 µm. The values for ten times the indentation depth (H_c^v) is still considerably lower than the sample thickness (210 µm) of the test sample. Therefore, the thickness of the sample satisfies the minimum thickness requirement to avoid thickness effects.

4.1.3.1 The effect of heat treatment on hardness

Isochronal heat treatments of the specimens were perfomed up to a temperature of 1200 °C, for 3 hours. Microhardness measurements were obtained and are shown in figure 4.1.3. The initial (as-cast) hardness for the specimen is 430 HV, decreasing to 390 HV after heat treatment at 800 °C. It further drops to 310 HV after heat treatment at 1000 °C. After heat treatment at 1050 °C the hardness is observed to increase relative to the 1000 °C heat treatment, to 345 HV, and further increases to 370 HV after heat treatment at 1070 °C. The hardness further increases to 400 HV at 1200 °C.

The specimens were also heat treated at 900 °C, 1000 °C and 1200 °C; for 168 hours and the hardness values were 349 HV, 310 HV and 114 HV respectively. The hardness for 3 hours and 168 hours heat treatment were the same for the temperatures below the transformation temperature. However, the hardness value was much lower for the 168 hour heat treatment than for the 3 hour heat treatment for the specimen heat treated at 1200 °C (which is above the transformation temperature).

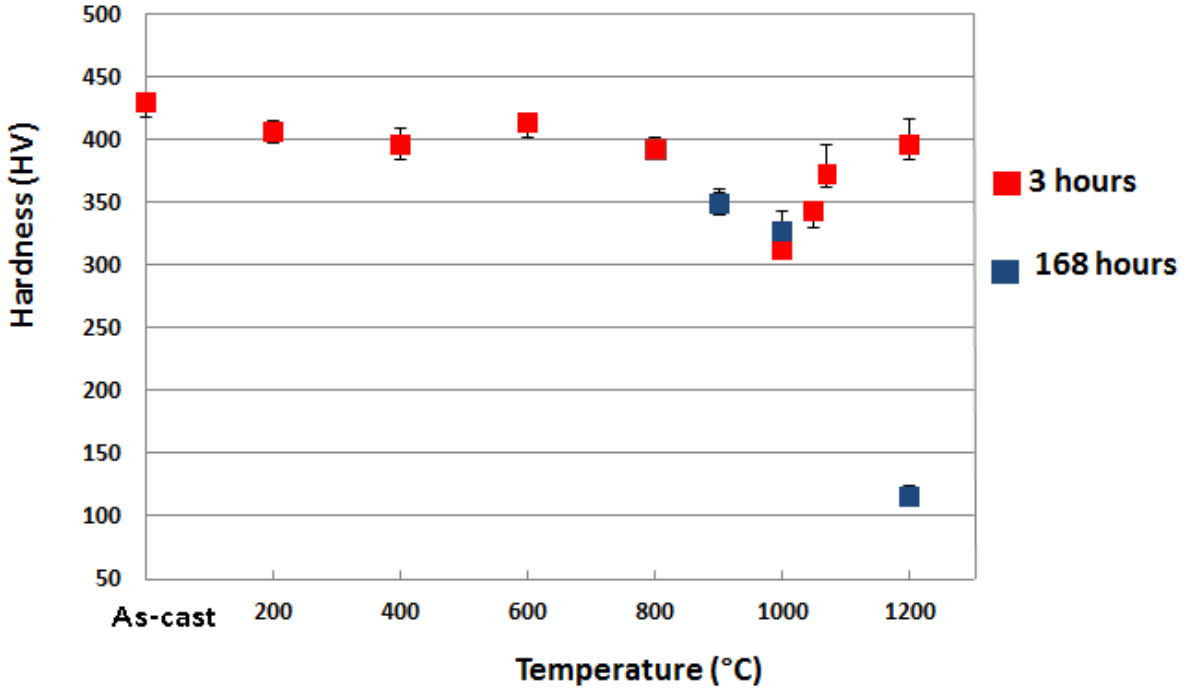

Figure 4.1.3: Hardness vs. heat treatment temperature for Pt 11 at. % Zr heat treated for 3 hours and 168 hours.

4.1.4 Metallography

Light micrographs of the Pt 11 at. % Zr specimens, heat treated at temperatures up to 1200 °C for 3 hours, are presented in this section.

4.1.4.1 The effect of heat treatment temperature on microstructure

Light micrographs of Pt 11 at. % Zr, after heat treatment at temperatures up to 1200 °C, are shown in figure 4.1.4a to 4.1.4g. The alloy appears to be single phase with no visible precipitates, for all heat treatment temperatures. The grain size is seen to be large, with no significant change in the grain size after heat treatment.

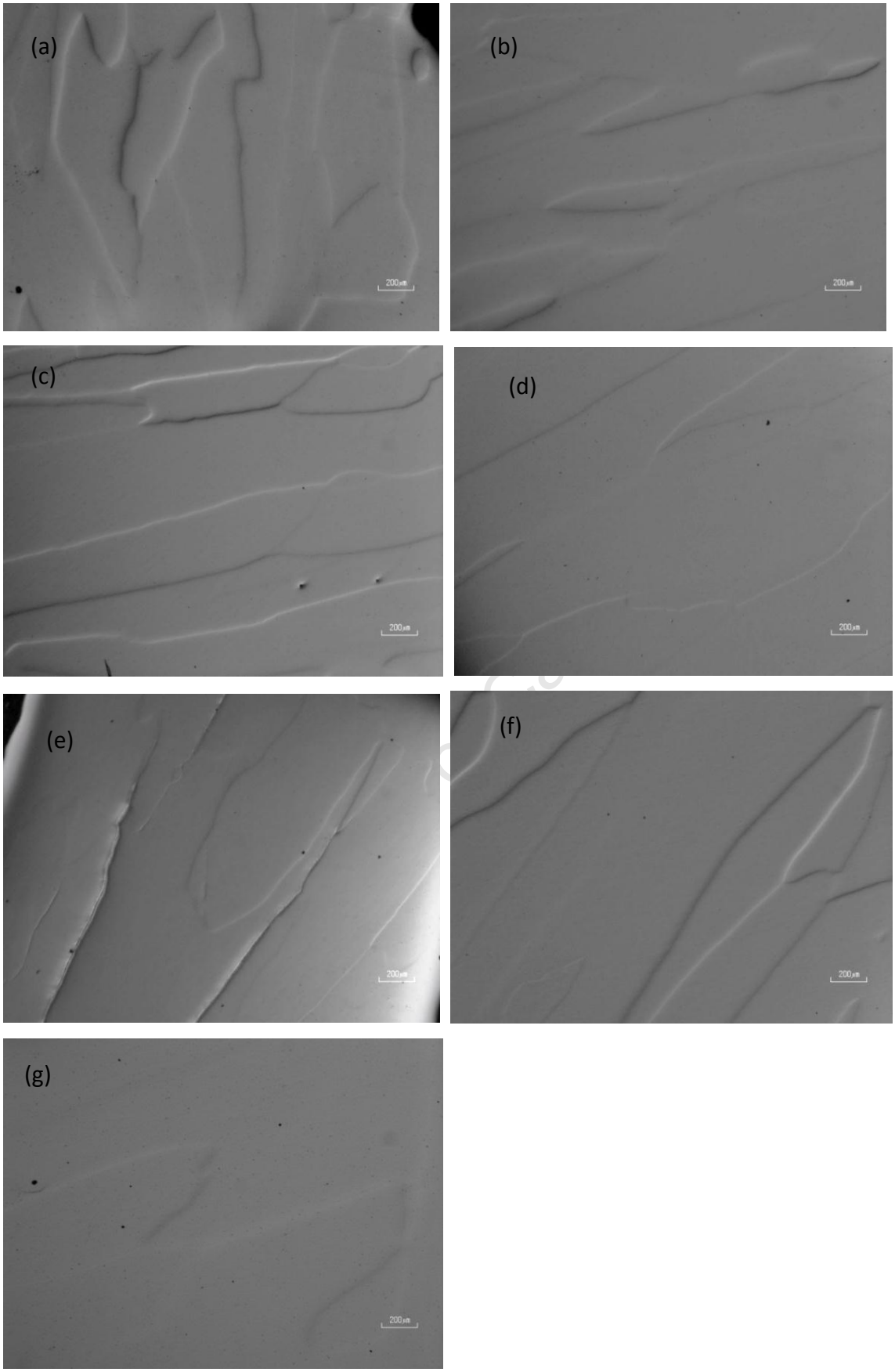

Figure 4.1.4: Light micrograph of Pt 11 at. % Zr for the (a) as cast initial condition and for the specimens heat treated at (b) 800 °C, (c) 900 °C, (d) 1000 °C, (e) 1050 °C, (f)1070 °C and (g) 1200 °C for 3 hours.

4.1.5 DSC Measurements

DSC measurements were obtained from a previously unheated specimen. The following heating profile was used. The specimen was heated to 1200 °C; (which was selected as it is above the predicted transformation temperature); at rate of 15 min/°C. The DSC curve obtained for the heating curve is shown in figure 4.1.5. An endothermic peak is observed at 1068.8 °C.

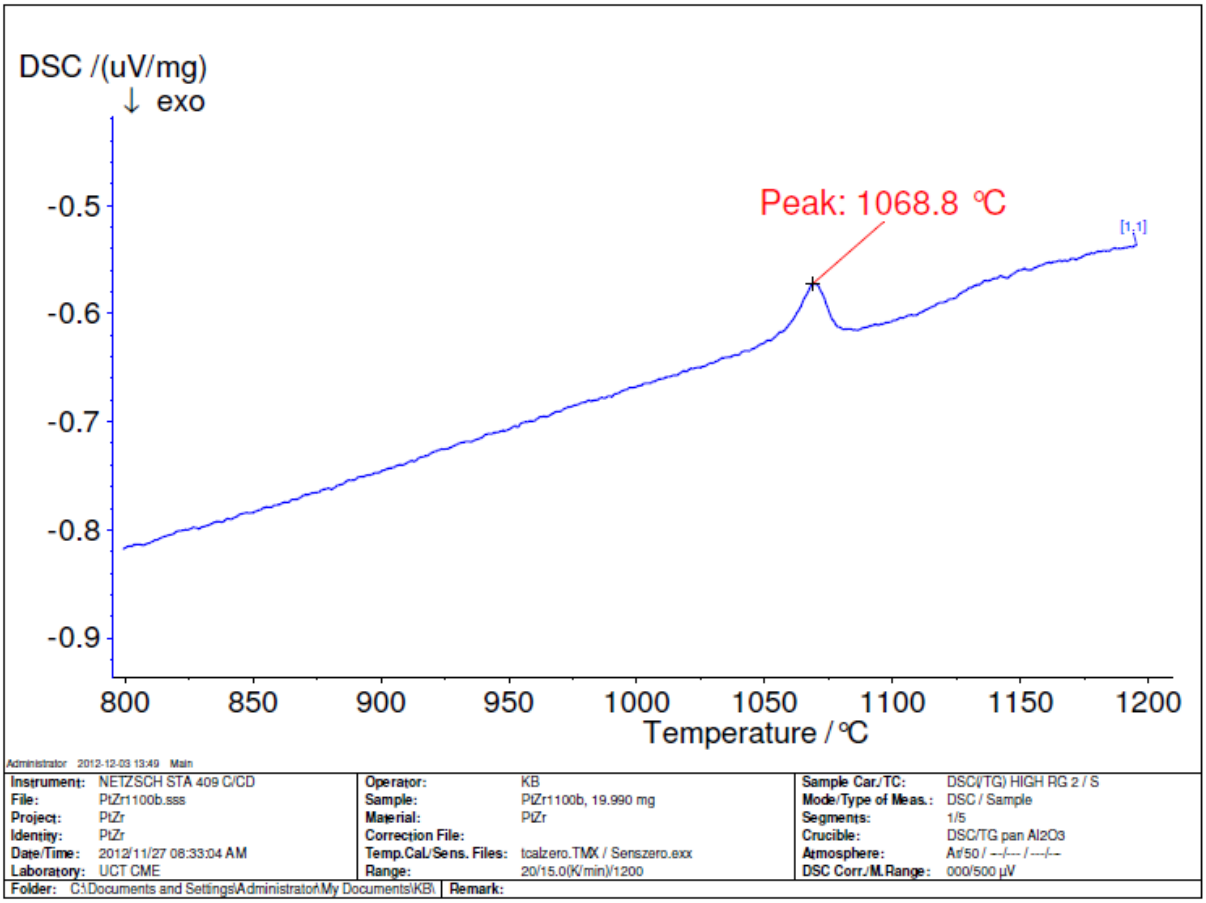

Figure 4.1.5: A DSC plot for the Pt 11 at. % Zr alloy showing the heating profile.

4.2 The platinum-Vanadium System

Platinum-vanadium results are presented in this section. Heat treatments were performed on Pt 11 at. % V specimens in two different media, namely, vacuum and 15 % hydrogen (-with 85 % argon by volume). TEM electron diffraction patterns are presented first, then dark field images followed by hardness measurements. Light micrographs are presented and finally, DSC measurements are also presented.

4.2.1 Electron Diffraction Patterns

Zone axis electron diffraction patterns are presented for Pt 11 at. % V alloys, with the following zone axes: $[00\text{-}1]_{fcc}$, $[0\text{-}11]_{fcc}$, $[\text{-}1\text{-}12]_{fcc}$ and $[0\text{-}13]_{fcc}$. It has been previously determined by Nxumalo and Lang[24] that Pt 11 at. % V undergoes an ordering transformation thereby forming ordered Pt_8V domains. The transformation temperature for this alloy was determined to be 810 ± 10 °C; therefore heat treatments were carried out at temperatures below 810 °C to ensure that Pt_8V was formed, which is seen to be the case. Electron diffraction patterns are shown in figure 4.2.1b to 4.2.1d, for heat treatment under both media.

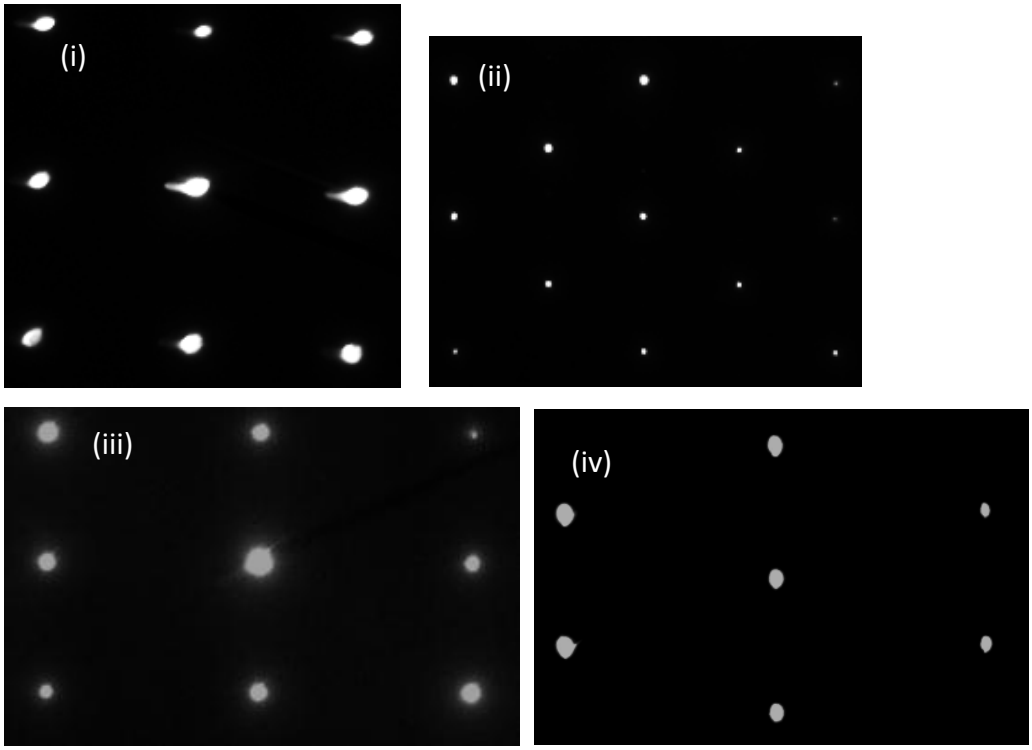

Figure 4.2.1a: Zone axis electron diffraction patterns for Pt 11 at. % V alloy for the initially deformed condition showing (i) [00-1]fcc, (ii) [0-11]fcc, (iii) [-1-12]fcc and (iv) [0-13]fcc zone axes, showing fundamental fcc reflections only.

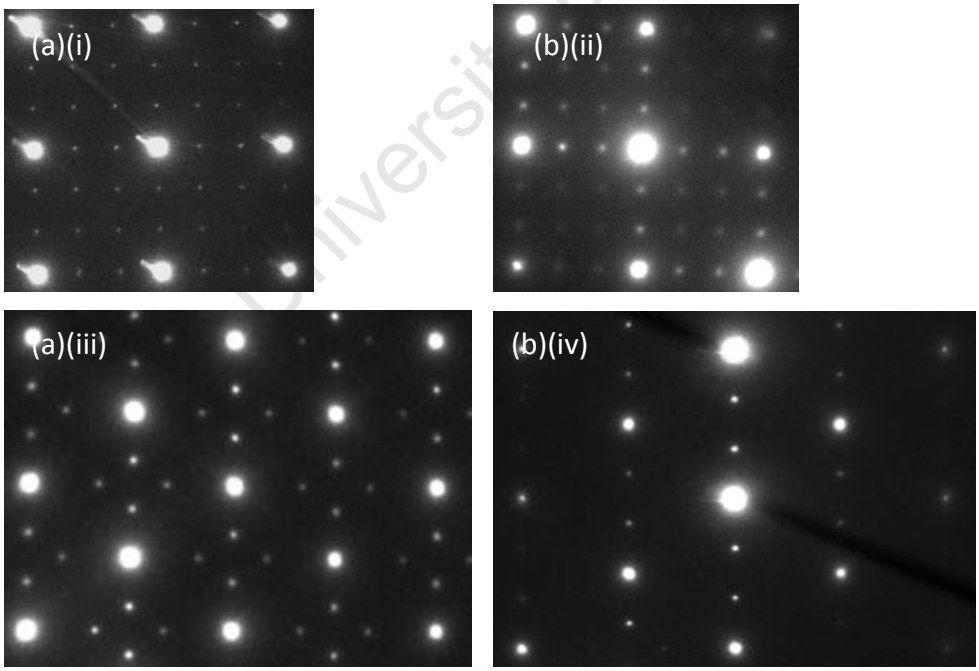

Figure 4.2.1b: Zone axis electron diffraction patterns from platinum-vanadium for (a) vacuum and (b) hydrogen heat treatment, at 500 °C for 3 hours, showing (i) [00-1]fcc, (ii) [0-01]fcc, (iii) [0-11]fcc and (iv) [0-11]fcc zone axes.

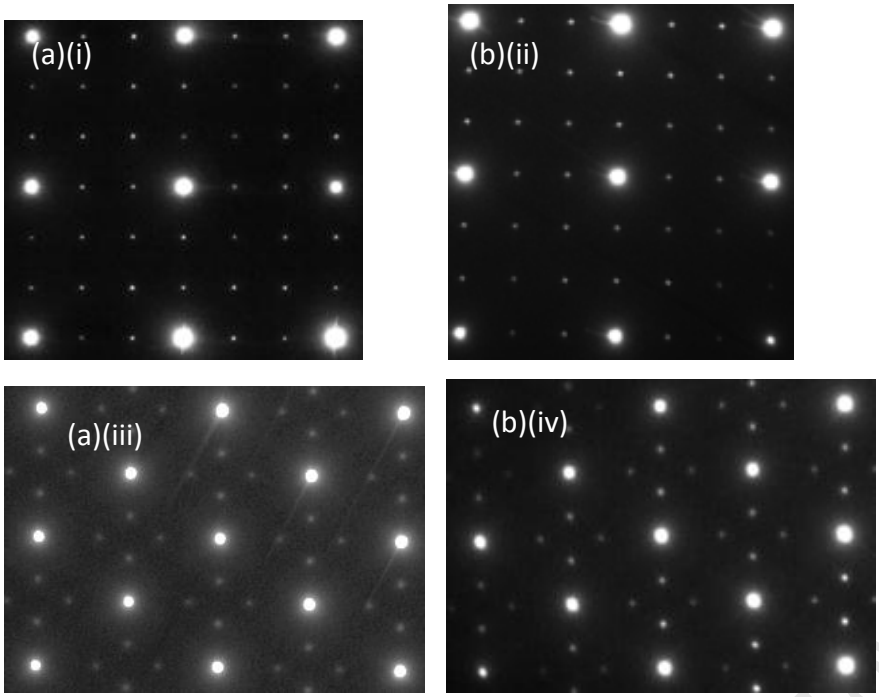

Figure 4.2.1c: Zone axis electron diffraction patterns for (a) vacuum and (b) hydrogen platinum-vanadium after a heat treatment of 600 °C for 3 hours showing (i) $[00\text{-}1]_{fcc,}$ (ii) $[00\text{-}1]_{fcc}$, (iii) $[0\text{-}11]_{fcc}$ and (iv) $[0\text{-}11]_{fcc}$ zone axes.

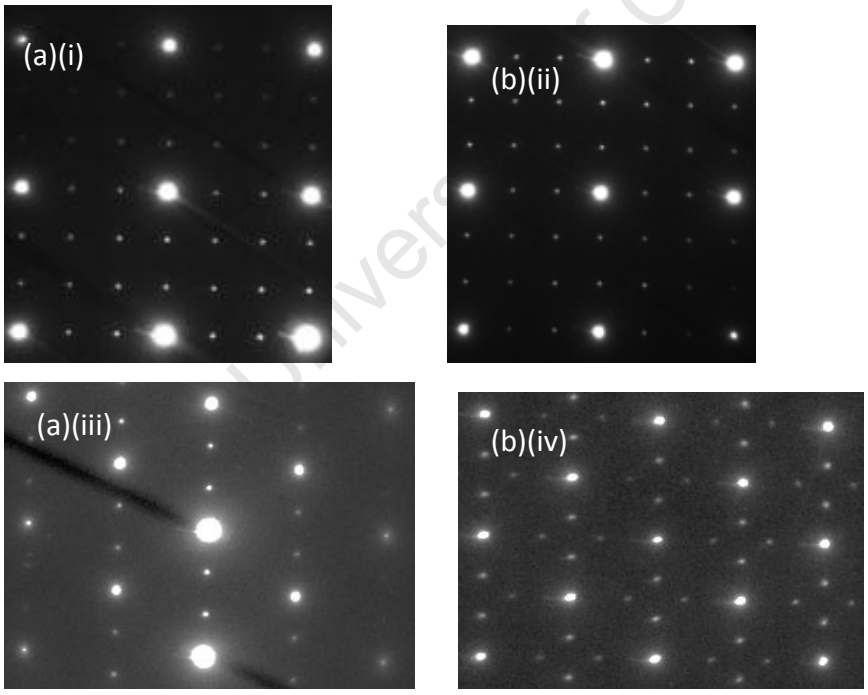

Figure 4.2.1d: Zone axis electron diffraction patterns for (a) vacuum and (b) hydrogen platinum-vanadium after a heat treatment of 700 °C for 3 hours showing (i) $[00\text{-}1]_{fcc}$, (ii) $[00\text{-}1]_{fcc}$, (iii) $[0\text{-}11]_{fcc}$ and (iv) $[0\text{-}11]_{fcc}$ zone axes.

4.2.2 TEM Dark Field Images

TEM dark field images were and obtained from the superlattice reflection arrowed in figures 4.2.2a to 4.2.2f.

4.2.2.1 The effect of heat treatment temperature and medium on domain size

After heat treatments of Pt 11 at. % V between 400 °C and 800 °C in two different media, the electron diffraction patterns indicate that the specimen is ordered. Dark field images of the ordered regions are presented in this section. The ordered domains are seen in bright contrast. The ordered domain size, for specimens heat treated in each medium at 500 °C, is about 5 nm in diameter. After heat treatment at 600 °C the ordered domains are about 10 nm in diameter. After heat treatment temperature of 700 °C, the ordered domains for both specimens significantly increased, to about 40 nm in diameter.

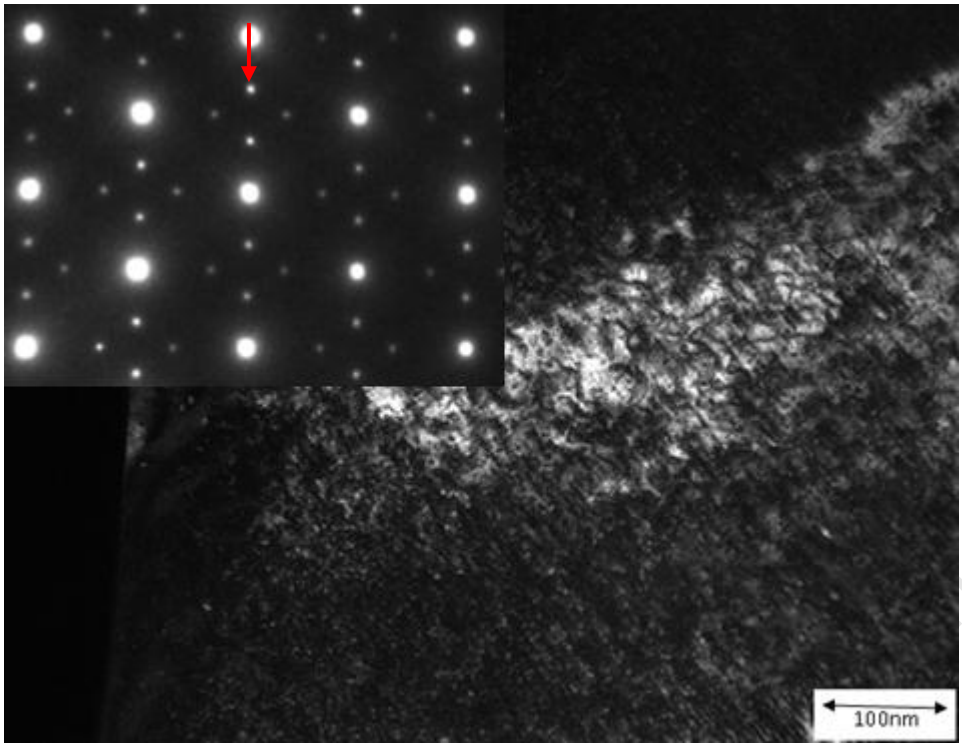

Figure 4.2.2a: Dark field image, obtained using the arrowed reflection, of 500 °C/3 hour/vacuum heat treated platinum 11 at. % vanadium, showing ordered precipitates in bright contrast.

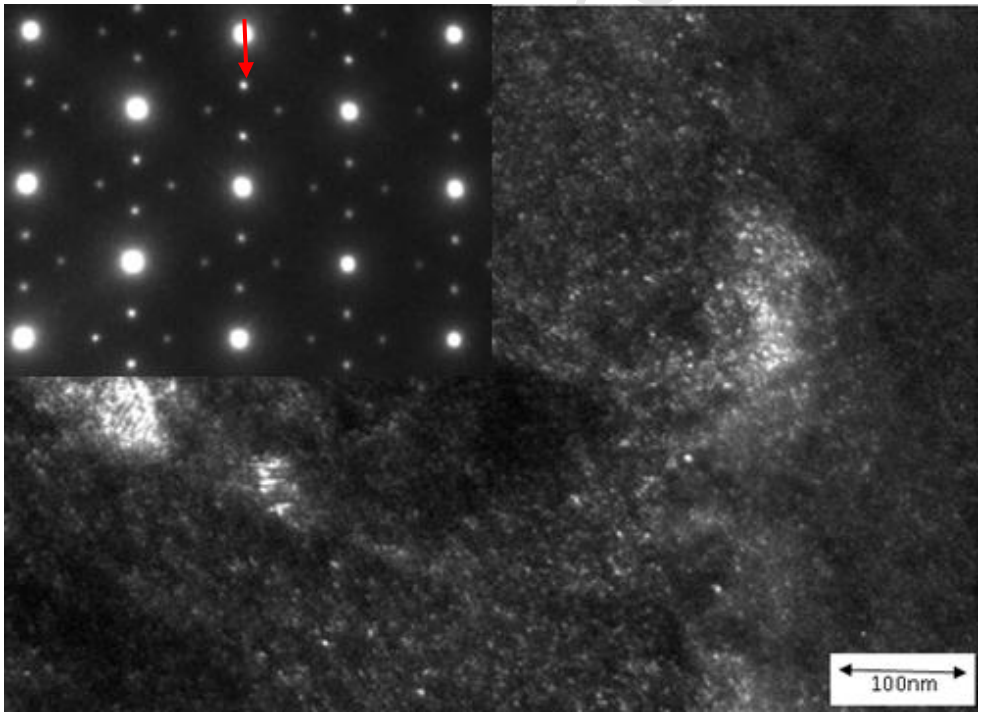

Figure 4.2.2b: Dark field image, obtained using the arrowed reflection of 500 °C/3 hour/hydrogen heat treated platinum 11 at. % vanadium, showing ordered precipitates in bright contrast.

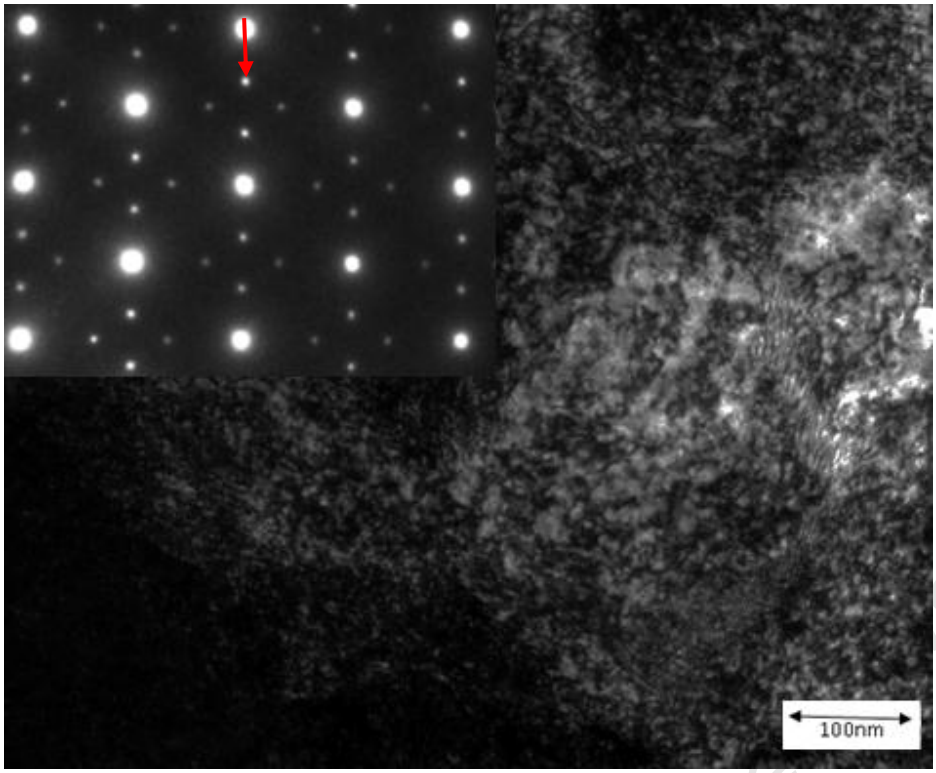

Figure 4.2.2c: Dark field image, obtained using the arrowed reflection, of 600 °C/3 hour/vacuum heat treated platinum 11 at. % vanadium, showing ordered precipitates in bright contrast.

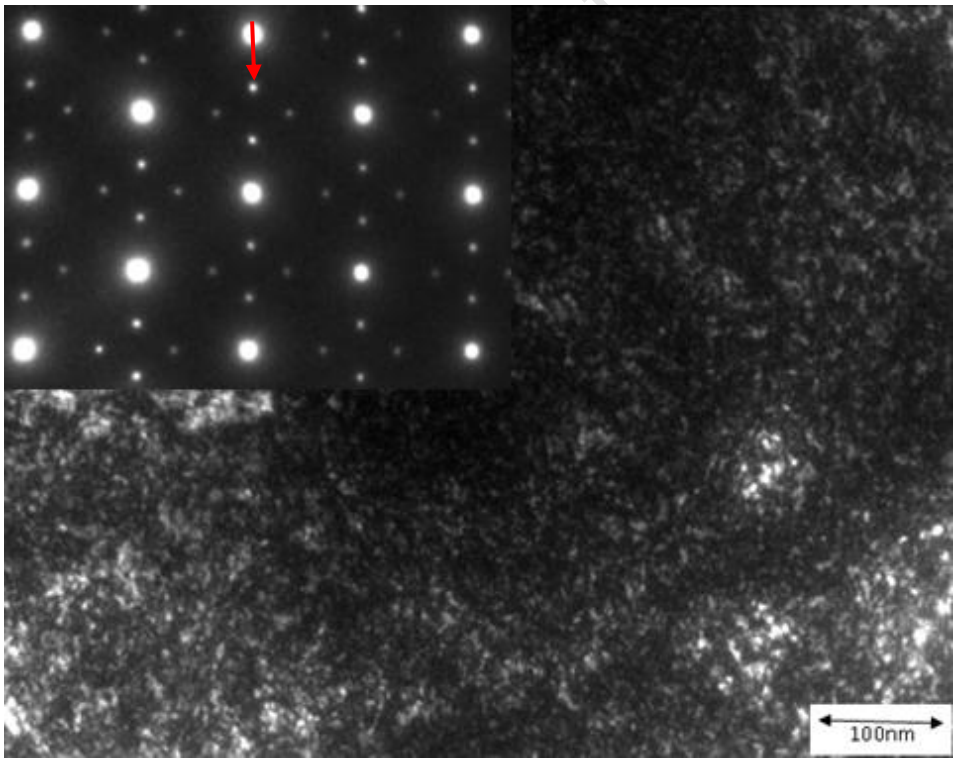

Figure 4.2.2d: Dark field image, obtained using the arrowed reflection, of 600°C/3 hour/hydrogen heat treated platinum 11 at. % vanadium, showing ordered precipitates in bright contrast.

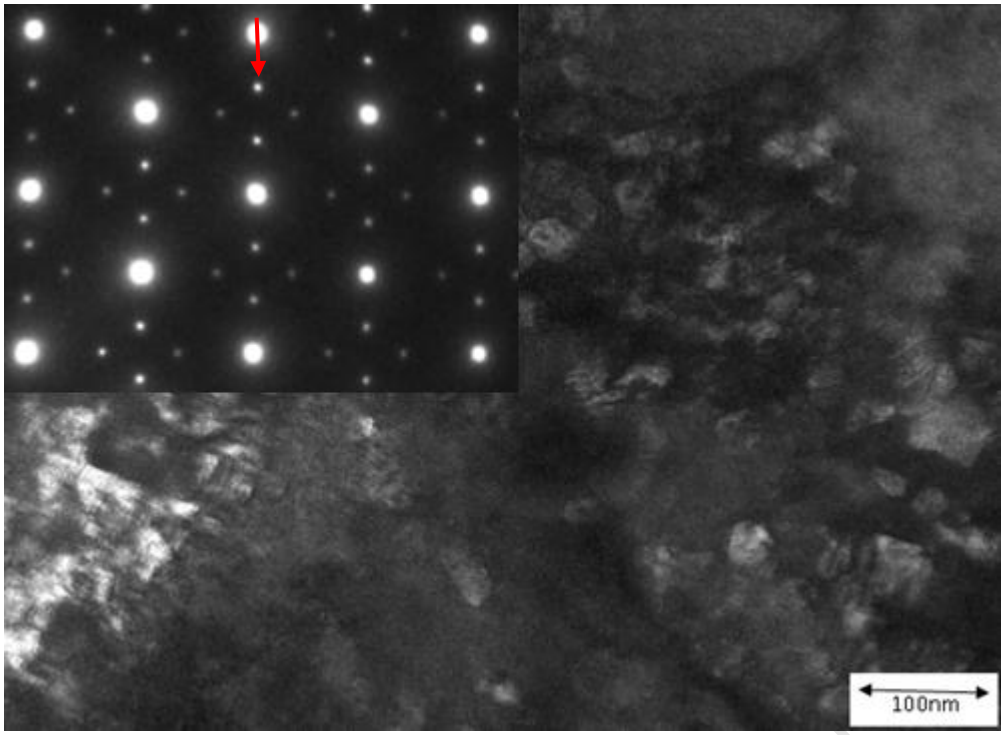

Figure 4.2.2e: Dark field image, obtained using the arrowed reflection, of 700°C/3 hour/vacuum heat treated platinum 11 at. % vanadium, showing ordered precipitates in bright contrast.

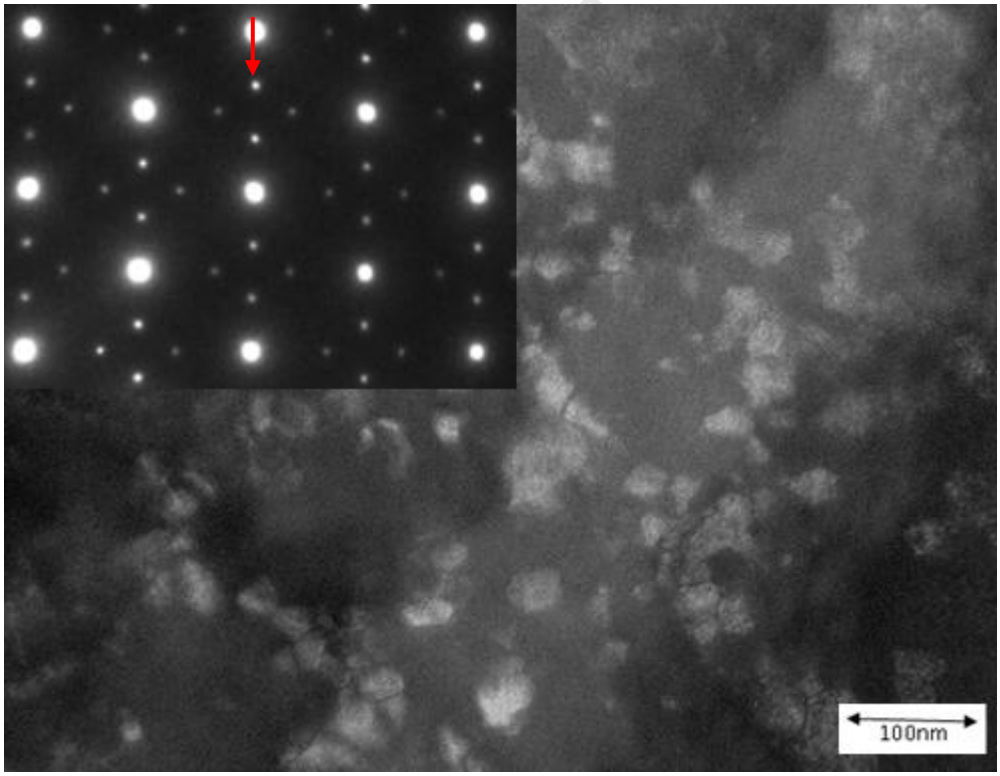

Figure 4.2.2f: Dark field image, obtained using the arrowed reflection, of 700 °C/3 hour/hydrogen heat treated platinum 11 at. % vanadium, showing ordered precipitates in bright contrast.

4.2.3 Hardness Measurements

Microhardness results, for the platinum-vanadium specimens heat treated in different media, were also obtained and are presented in this section. Each heat treatment was conducted twice and 10 hardness measurements were taken for each heat treatment temperature for the two media. Referring to section 4.1.3, the thickness of the platinum-vanadium samples did not affect the hardness measurements obtained.

4.2.3.1 The effect of heat treatment temperature and heat treatment medium on hardness

The hardness of the initially deformed specimen was about 355 HV. After heat treatment, the hardness increased to about 430 HV for the temperatures up to 700 °C. The hardness of the isochronal heat treatment specimens below the transformation temperature is shown to be higher than the hardness above the transformation temperature for both media: the hardness decreased from about 430 HV in the ordered state to about 230 HV in the disordered state. The hardness of the specimens heat treated in 15 % hydrogen is closely similar to that of the specimens heat treated in vacuum, for the same heat treatment temperature and time.

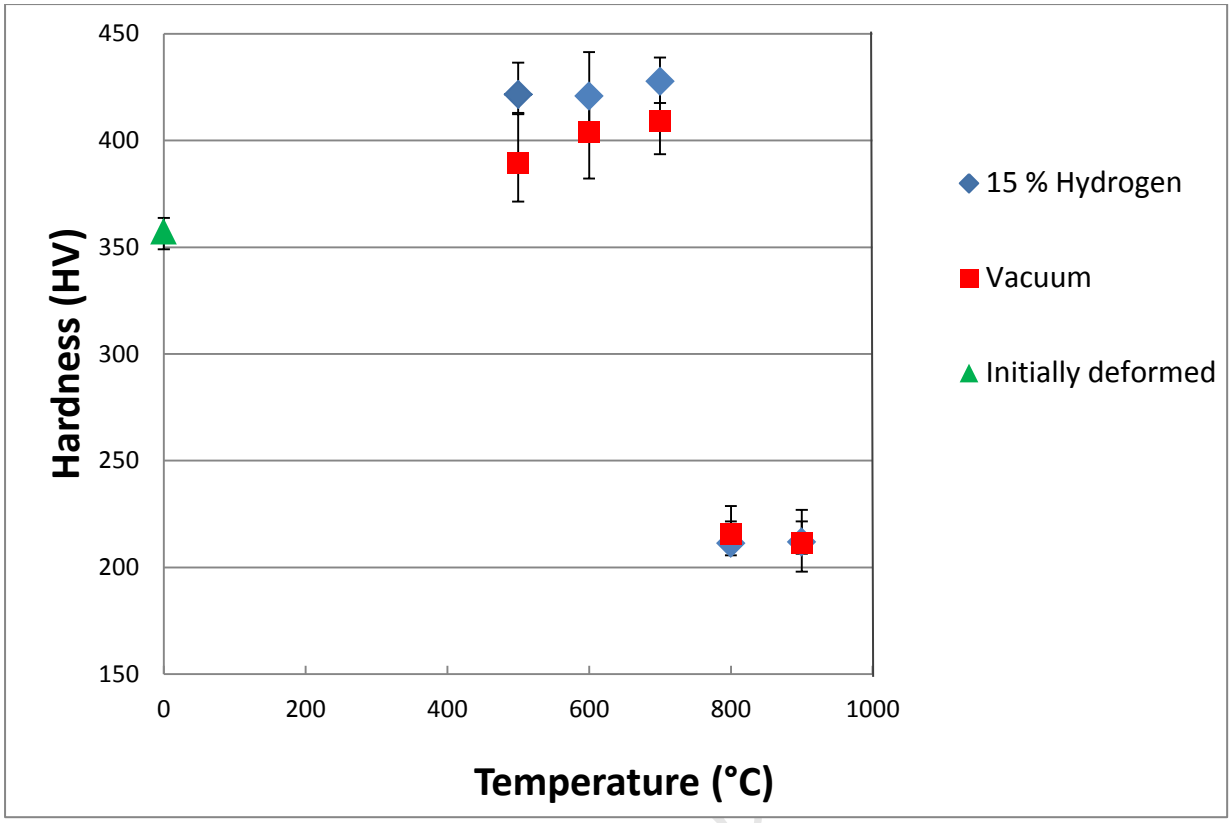

Figure 4.2.3: Hardness vs. Heat treatment temperature for both specimens heat treated in 15% hydrogen medium and a vacuum medium for the platinum-vanadium alloy.

4.2.4 Metallography

4.2.4.1 The effect of heat treatment temperature and heat treatment medium on microstructure

The microstructure of the initially deformed platinum 11 at. % vanadium specimen shows heavily deformed grains, as shown in figure 4.2.4a. The grains are elongated in the rolling direction as shown by the arrow. The specimen heat treated at 750 °C for 3 hours (for both conditions) still show a heavily deformed microstructure with elongated grains. After heat treatment at 850 °C, the microstructure shows recrystallized grains as shown in figure 4.2.4e and figure 4.2.4f.

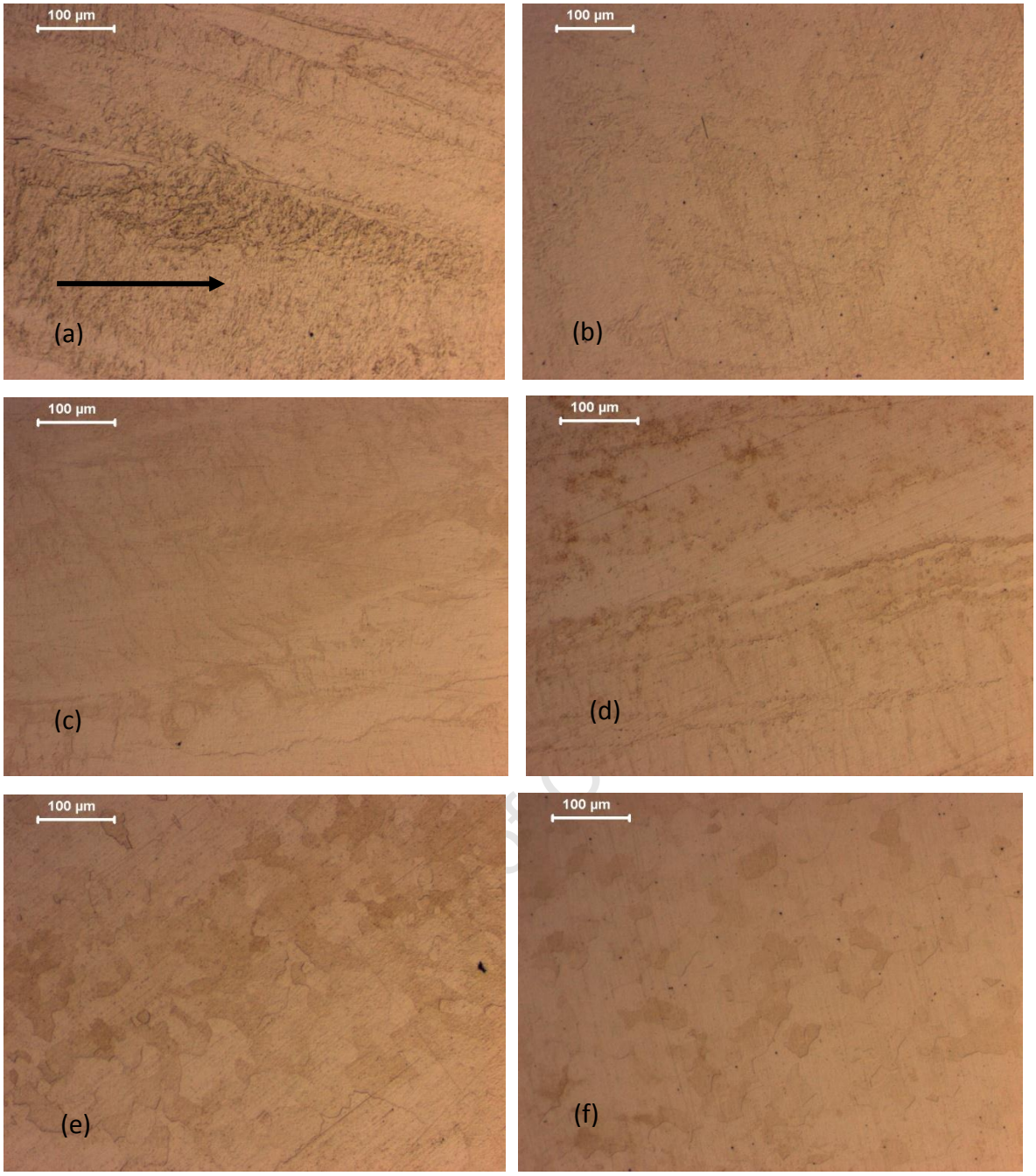

Figure 4.2.4: Light micrographs of Pt 11 at. % V for the (a) initially deformed specimen and for the specimens heat treated for 3 hours at (b) 400 °C in vacuum, (c) 750 °C in vacuum, (d) 400 °C in 15% hydrogen, (e) 850 °C in vacuum and (f) 850 °C in 15% hydrogen.

4.2.5 DSC Measurements

After a heat treatment at 700 °C for 3 hours of the specimens in 15 % hydrogen and in vacuum, DSC measurements were obtained. The following profile was used for both specimens: The specimen was heated from room temperature to 1000 °C at the rate of 15 min/°C.

4.2.5.1 The effect of heat treatment medium on the DSC curve

The DSC curves for specimens of platinum 11 at. % vanadium heat treated in different media, show some similarities. Figure 4.2.5 shows the results obtained after a heat treatment of 700 °C for each specimen. The red curve illustrates the results obtained for the hydrogenated specimen and the black curve illustrates the results obtained for the vacuum heat treated specimen. The DSC curves shows exothermic peaks at 431.6 °C and at 440.5 °C for the specimen heat treated in hydrogen and vacuum respectively.

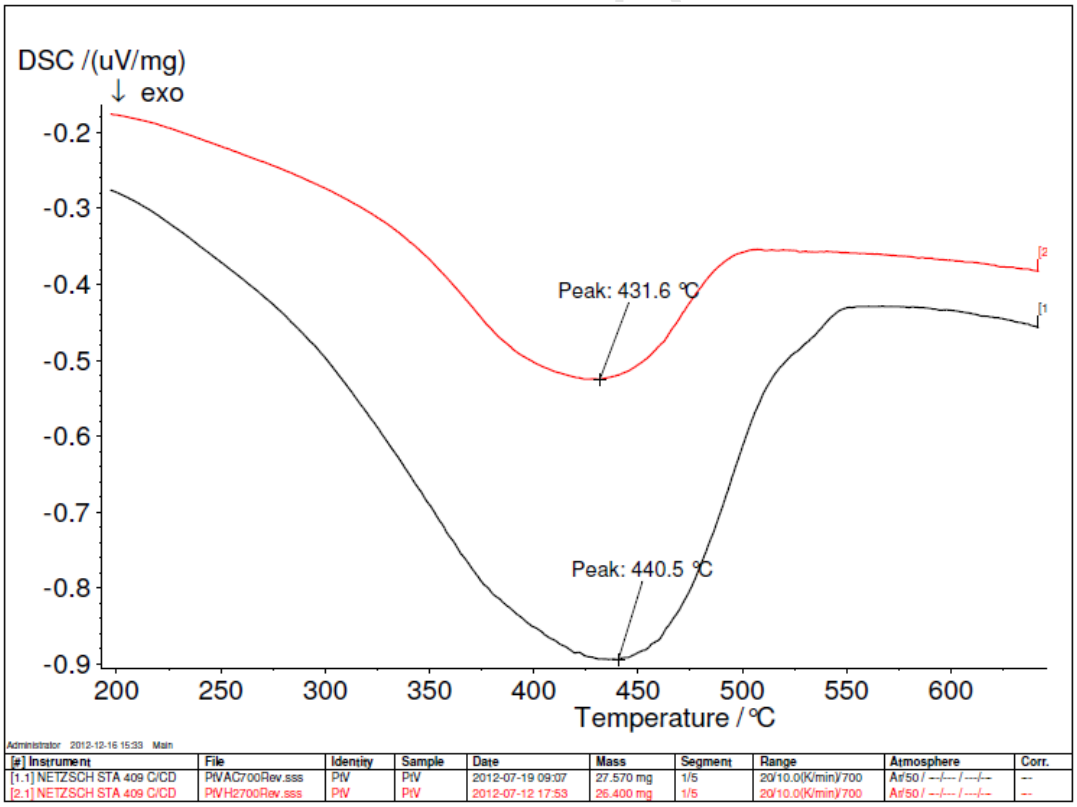

Figure 4.2.5: DSC heating curve of the Pt 11 at. % V specimens obtained after a heat treatment of 700 °C for each heat treatment medium.

5. DISCUSSION

This Chapter discusses the results presented in Chapter 4. The order/disorder temperature and the factors that affect the kinetics of the ordering transformation of the Pt_8Zr phase are discussed first, followed by the effect of ordering on hardness. The effect of heat treatment on microstructure is considered and finally, DSC measurements of the Pt 11 at. % Zr alloy are discussed.

In section 5.2, the formation of the Pt_8V domains is discussed first, followed by the effect of heat treatment temperature and medium on the domain size. The effect of the heat treatment medium on hardness, microstructure and on DSC measurements is also discussed.

5.1 Formation of Pt_8Zr and Determination of T_c

The initial as-cast Pt 11 at. % Zr specimen, together with the specimens heat treated at temperatures up to 1070 °C, exhibited additional reflections in zone axis electron diffraction patterns. Figures 4.1.1b to 4.1.1f show electron diffraction patterns consisting of not only the fundamental fcc reflections but also additional reflections. These electron diffraction patterns are consistent with those of Pt_8V that were simulated [32] and observed by Schryvers and co-workers [24]. The predicted ordering in this Pt-Zr alloy [26]; the 8:1 stoichiometry of the alloy; and the additional reflections in diffraction patterns which are consistent with other A_8B alloys, together demonstrate the presence of Pt_8Zr. It can therefore be concluded that up to a temperature of 1070 °C, the equilibrium state of the Pt 11 at. % Zr alloy is ordered.

The electron reflection patterns obtained from the specimen heat treated at 1090 °C exhibited only the fundamental fcc reflections, and did not contain superlattice reflections. The alloy is therefore disordered at 1090 °C. These results suggest that the T_c for Pt_8Zr is above 1070 °C and below 1090 °C.

5.1.1 Kinetics of The Pt_8Zr Ordering Transformation

The Pt_8Zr ordering transformation is expected to be a diffusional process. It involves substitutional diffusion, with the presence of vacancies [33] as a prerequisite. Since atomic movement and vacancy concentration both increase with increasing temperature, an increase in temperature is expected to result in an increase in diffusion and consequently, in the transformation rate.

The A_8B structures are expected to require an excess of vacancies to form, particularly the platinum-based Pt_8X alloys [36]. Typically, Pt_8X alloys need to be deformed, or quenched from above T_c, to provide a sufficient vacancy concentration for formation of ordered structures. The Pt 11 at. % Zr as-cast specimen however exhibited the Pt_8Zr phase without prior deformation, or prior quenching from high temperatures, which suggests that the kinetics of the Pt_8Zr formation are very fast. This may account for the fact that this ordered structure was observed by Meschter and Worrell [26] in 1977, whereas other Pt_8X (Pt_8V and Pt_8Ti) alloys were not reported until more recently.

Impurities (trace elements) are known to affect the phase transformations of alloys and elements. Depending on the impurities, the kinetics of phase transformations can be affected differently. For example, in titanium, impurities block the α to ω martensite transformation [41]. Due to the possibility of the platinum-zirconium button consisting of impurities that might have been introduced during elemental feed, they might have enhanced the ordering kinetics as impurities alter the phase transformations of alloys differently. Hence the Pt 11 at. % Zr alloy behaves differently from other Pt_8X alloys.

5.1.1.1 Nucleation and growth

The formation of Pt_8X ordered domains occurs by nucleation followed by growth. There are two types of nucleation, namely homogeneous and heterogeneous nucleation. Heterogeneous nucleation involves the presence of preferential nucleation sites which are not required for homogeneous nucleation, in which nucleation is uniformly distributed. For heterogeneous nucleation, the nucleation sites are usually non-equilibrium defects such as vacancies, dislocations, inclusions, grain boundaries, stacking faults and free surfaces.

Heterogeneous nucleation accordingly results in a non-uniform distribution of the second phase in the matrix [34].

In the present work, TEM dark field images (section 4.1.2) show that the ordered domains have a uniform distribution in the matrix which suggests that nucleation is homogeneous. The Pt_8Zr phase readily nucleates without prior introduction of nucleation sites; it was observed in the initial as-cast state. This is consistent with the conclusions of Ardell [2] that not all A_8B alloys require the presence of excess vacancies to form.

Pt 11 at. % Zr shows nucleation of the Pt_8Zr phase in the as-cast state of the alloy. The Pt_8Zr domains range from 5 to 10 nm in diameter, from the as-cast state to the specimens heat treated at 1070 °C or for 600 hours at 1000 °C. This shows that higher temperature and longer heat treatment times do not accelerate the growth of the Pt_8Zr phase. Nucleation of the ordered phase is therefore rapid, but growth was not observed thereafter, even at elevated temperatures. The effect of longer times will be considered in section 5.1.3.

5.1.2 The Effect of Ordering on Hardness

Previously, it has been observed that ordering increases the hardness of the Pt_8X alloys [36], particularly in initially deformed specimens. The Pt 11 at. % Zr alloy starts off with a hardness of 430 HV in the as-cast state, in which the alloy has been shown to be ordered by electron diffraction (section 4.1.1). The condition of specimens before heat treatment is thus already ordered. After heat treatment up to 800 °C the hardness decreases by around 40 HV, decreasing more rapidly to 310 HV after heat treatment at 1000 °C and changing to 370 HV after heat treatment at 1070 °C. These values, i.e. over a range of 310 HV – 430 HV, are all for specimens which exhibit order. Heat treatment at 1200 °C for 3 hours, which results in disorder, gives a measured value of 392 HV.

The dark-field images shown in Section 4.1.2 suggest that a mixed order/disorder structure is present in all specimens heat treated up to 1070 °C, with ordered Pt_8Zr domains present in a disordered matrix. This configuration, analogous to a small precipitate in a matrix, is expected to lead to high hardness, which may decrease as precipitate (or domain) size increases.

For example, in the Pt_8V alloy, it has been found that the hardness decreases with an increase in domain size [36]. In the Pt 11 at. % Zr alloy, however, there is little change in the domain size as heat treatment temperature, or time, changes. The only significant change with heat treatment is for the specimen heat treated at 1200 °C, which is observed to be disordered.

The hardness for the specimen heat treated for 600 hours at 1000 °C was approximately 146 HV which was significantly less than the hardness of 310 HV for the specimen heat treated for 3 hours at the same temperature. This decrease in hardness might be due disordering that might have taken place (TEM can be used to investigate this change).

The hardness of ordered Pt 11 at. % Zr specimens varies in the range 310 HV – 430 HV, with disordered Pt 11 at. % Zr lying in the same range with a value of 392 HV after 3 hours. Little or no change in the ordered configuration thus occurs in association with a 120 HV variation in hardness; whereas an apparent order/disorder transformation results in an insignificant change in hardness.

Even though the specimen was disordered at 1200 °C, the hardness was still in the same range of the ordered specimen's hardness. For this system, it appears as though the hardness is independent of the order/disorder state of the specimen. Baker [43] reported that strongly-ordered alloys soften during recovery while weakly-ordered alloys either soften or harden depending on whether annealed below or above the T_c. An initially deformed, ordered alloy is likely to recrystallize more rapidly than an undeformed disordered alloy because the stored energy associated with dislocations is higher in the ordered state. Hence, (referring to section 5.1.3), recovery was more likely to have taken place and caused it to harden after the transformation temperature.

The specimens heat treated at 3 hours and 168 hours for the same temperature showed the same hardness values below the transformation temperature, but the specimens heat treated above the transformation temperature (1200 °C), showed a difference of approximately 270 HV for the same heat treatment temperature. This significant decrease suggests that at 1200 °C, the specimen is not at equilibrium after 3 hours; and may still be progressing towards equilibrium after 600 hours.

5.1.3 The Effect of Heat Treatment on Microstructure

Section 4.1.4 shows micrographs obtained for the as-cast specimen and specimens heat treated up to 1200 °C for the Pt 11 at % Zr alloy. The specimens, all exhibit a single phase and the grains were elongated.

The driving force for recrystallisation is the internal energy and surface energy [35] of dislocations and grain boundaries. Therefore, for a change in grain size to occur, there must be adequate energy present to drive recrystallisation and grain growth. Prior to heat treatment of the specimens, no deformation was introduced to raise this internal energy; as expected then, no grain growth was observed in the microstructures.

5.1.4 The Effect of Heat Treatment Time on Ordered Domains

The TEM results showed the presence of Pt_8Zr in the as-cast state. This suggests that the kinetics of the Pt_8Zr formation were very fast, the ordered phase nucleating immediately after solidification. To further determine the thermodynamic stability of the Pt_8Zr phase, long heat treatments were carried out. The long heat treatment times should be long enough and heat treatment temperature high enough to allow diffusion to occur leading to completion of the Pt_8Zr transformation. The ordered domains for specimens heat treated at 1000 °C for 3 hours and for 600 hours showed no difference in the domain size. This is not consistent with similar alloys, for instance Pt 11 at. % V, in which the Pt_8V phase has been shown to increase in size with an increase in heat treatment time [36].

Therefore, the growth kinetics of the Pt_8Zr domains appear to be rather slow, which suggests for domain growth and achievement of equilibrium, a higher heat treatment temperature (but below T_c) and/or much longer heat treatment times may be necessary.

Above 1070 °C, electron diffraction patterns do not exhibit any additional reflections, suggesting that disordering has taken place completely.

5.1.5 DSC and Ordering

For this study, the differential scanning calorimetry technique was used to determine the temperature of any phase change. A peak is expected at the order/disorder temperature, endothermic on heating (as the specimen disorders at T_c) and exothermic on cooling (as the

specimen orders on undercooling below T_c). Section 4.1.5 shows the results obtained for the DSC measurements.

An endothermic disordering peak was observed on heating, at 1068 °C for the Pt 11 at. % Zr alloy, indicating that above this temperature the alloy becomes disordered. This temperature is consistent with the results shown by the TEM diffraction patterns in section 4.1.1, which show that the alloy is ordered up to about 1070 °C. The transformation temperature for the Pt 11 at. % Zr is concluded to be about 1070 °C.

5.2 Formation of Pt_8V Domains

Previously [36], it was observed that the Pt_8V phase was formed for specimens heat treated up to a temperature of 810 °C. Deformation followed by a homogenization heat treatment and finally quenching from above 810 °C were the processes performed prior to the isochronal heat treatments in the present work, and previously reported by Nxumalo and Lang [21]. It was observed that all these processes were necessary to drive nucleation and growth of ordered domains. Unlike the platinum-zirconium system, for ordering to occur, energy is required to drive the kinetics of the ordering transformation in order to reach equilibrium. Isochronally heat treated specimens show ordering (of disordered specimens prepared as described above) to occur from a temperature of 300 °C to 810 °C.

Section 4.2.1 shows the electron diffraction patterns obtained for the Pt 11 at. % V alloy. TEM diffraction patterns of specimens isochronally heat treated at temperatures of 500 °C, 600 °C and 700 °C showed not only fundamental fcc reflections but also the Pt_8V superlattice reflections, for specimens heat treated in vacuum or in a hydrogen atmosphere. The formation of Pt_8V in this temperature range was consistent with the findings of Nxumalo and Lang [21] who reported that the Pt_8V domains are formed at temperatures between 300 °C and 810 °C.

5.2.1 The Effect of Heat Treatment Medium on Domain Size

Pt 11 at. % V specimens heat treated in two media (15 % hydrogen and vacuum atmosphere) were investigated. Section 4.2.2 shows the results obtained for the TEM dark field images, for specimens heat treated at 500 °C, 600 °C and 700 °C for both media. The ordered domains are shown in bright contrast. The domain size for the specimen heat

treated at 500 °C and 600 °C for both media are approximately 5 nm in diameter. In the present work, the ordered domains for the specimen heat treated at 700 °C, are approximately 40 nm in size for both heat treatment media. The ordered domains thus grow with elevated temperature heat treatment, but show no significant difference resulting from different heat treatment media.

5.2.2 The Effect of Heat Treatment Medium on Hardness

Section 4.2.3 shows the hardness values obtained for both heat treatment media. The initial hardness was approximately 355 HV, which was consistent with hardness values of 355 HV obtained by Nxumalo *et al*. [3]. After isochronal heat treatments for the temperatures between 500 °C and 700 °C, the hardness increased to approximately 430 HV in the present study. The hardness increase is due to ordering that occurred at these temperatures as shown by the electron diffraction patterns in section 4.2.2. The electron diffraction patterns and TEM dark field images show the presence of the Pt_8V phase. The hardness for both media was the same for the specimen heat treated at 500 °C, 600 °and 700 °C; this consistent with previous studies [3].

After a heat treatment at 800 °C and 900 °C, the hardness decreased to approximately 230 HV for both heat treatment media. It was previously [16] determined that the transformation temperature of this alloy is 810 ± 10 °C, thus the decrease in hardness is apparently due to disordering of the alloy. However, the hardness for both specimens was the same below and above the transformation temperature. Therefore, heat treatment medium does not affect the hardness of the Pt 11 at. % V alloy for this particular hydrogen concentration (15 % hydrogen and 85 % Argon by volume).

5.2.3 The Effect of Heat Treatment Medium on Microstructure

The microstructures obtained for Pt 11 at. % V heat treated in both media are shown in section 4.2.4. The microstructure for the specimens heat treated below the transformation temperature is those of heavily deformed grains. This is due to the button being heavily cold rolled inducing dislocations. The grains are aligned in the rolling direction as shown by figure 4.2.4a. This is consistent with the previous results by Nxumalo *et al.* [3]. The microstructures obtained were the same for both heat treatment media. At 850 °C, which is above the

transformation temperature, the microstructures for both media shows recrystallized grains as shown in figure 4.2.4e and figure 4.2.4f. These recrystallized grains are consistent with the recrystallized grains observed at 900 °C and 1000 °C [3]. The heat treatment medium does not have an effect on the microstructure.

Baker [43] reported that recrystallization and grain growth are dramatically reduced by atomic ordering which is associated with a reduction in grain boundary mobility. Below the transformation temperature, the kinetics are much slower, particularly due to the ordered nature of the grain boundaries. Figure 4.2.4e and figure 4.2.4f are consistent with recrystallization and disorder. Therefore, the decrease in hardness for the specimen heat treated at 800 °C for both media, can be associated with the onset of recrystallization.

5.2.4 The Effect of Heat Treatment medium on DSC Measurements

DSC measurements for both media are shown in figure 4.2.5. The DSC curves show exothermic peaks at 431.6 °C and at 440.5 °C for the specimen heat treated in hydrogen and vacuum respectively. Since these specimens were being heated in a temperature range in which order is the stable configuration (T_c for this system ≈ 810 °C), ordering is expected to occur. Both specimens started in the ordered condition (heat treated below T_c); further ordering occurs during the DSC test, as indicated by the broad, shallow peaks observed above 400 °C, when both vacancy concentration and atomic mobility allow further rearrangement of atoms. The peaks for both heat treatment media are observed to occur at approximately the same temperature; the heat treatment medium thus has little effect on the temperature at which the ordering transformation occurs.

Due to the previously established transformation temperature for the platinum-vanadium of 810 °C, an endothermic disordering peak is expected for the two specimens at approximately 810 °C. But this is not the case at discussed above. This could be due to the fact that some of the vanadium oxidised to form vanadium pentoxide (V_2O_5 – brown/yellow solid) as the crucibles had yellow residue after the DSC was performed. Therefore, this might have changed the composition of the alloy and the results obtained were for a different alloy composition.

6. CONCLUSIONS

Pt 11 at. % Zr undergoes an ordering transformation thereby forming the Pt_8Zr phase. The homogenous nucleation of the Pt_8Zr ordered phase is rapid but the growth is very slow. The ordered domains are approximately 5 to 10 nm in size for the as-cast specimen, the specimens heat treated for 3 hours and for the specimen heat treated at 1000 °C for 600 hours. The transformation temperature (T_c) for the Pt_8Zr is 1070 ± 10 °C as shown by the electron diffraction results.

The Pt_8V superlattice is observed to occur for the Pt 11 at. % V specimens heat treated at 500 °C, 600 °C and 700 °C for specimens heat treated in two different media (15 % hydrogen and vacuum atmosphere). The ordered domains were approximately 5 nm, 10nm and 40 nm in size for heat treatment at these temperatures. Hydrogen had no effect on the hardness results, microstructure analysis or DSC measurements. This could be due to one of two reasons. The atmosphere used for the hydrogenation was not effective in promoting hydrogenation or hydrogen does indeed not affect the hardness, microstructure and the growth of the ordered domains.

Therefore the following hypotheses are rejected.

- Pt_8Zr phase will be formed with a T_c between 827 and 1027 °C, which was obtained to be 1070 °C.
- The hardness of the Pt 11 at. % Zr will increase with the formation of the Pt_8Zr phase.
- Hydrogen will enhance the ordering kinetics of the Pt 11 at. % V alloy.

7. RECOMMENDATIONS

i. Pt 11 at. % Zr displays brittle behaviour in cold work; hot forging exposes the alloy to contamination, and hot compression does not suppress the brittle nature of the alloy. Deformation of such alloys is accordingly not advised prior to the heat treatment process.

ii. Due to the brittleness of the alloy, spark erosion is recommended to extract the 3 mm TEM samples.

iii. 15 % hydrogen (85 % Argon by volume) and vacuum atmosphere was used to investigate the effect of heat treatment media on ordering for the Pt 11 at. % V alloy. There was no effect observed for this hydrogen concentration; it may be useful to conduct experiments at a higher hydrogen concentration. (Due to safety regulations, the allowable hydrogen concentration analysed was 15 %).

iv. TGA (thermo-gravimetric analysis) can be used to measure the amount of hydrogen absorbed due to mass gain.

REFERENCES

[1] R. S. Irani, The thermodynamics and mechanisms of ordering systems, Contemp. Phys. 13 (1972) 559-583.

[2] J. S. Faulkner, R. G. Jordan, Formation and stability of A8B phases in Ni, Pd and Pt-base alloys, Experimental and Theoretical Perspectives. 256 (1994) 93-102.

[3] S. Nxumalo, M. P. Nzula, C. I. Lang, Order hardening of Pt_8X alloys, Mater, Sci. Eng.A. 445-446 (2007) 336-340.

[4] J. I. Qazi, O. N. Senkov, J. Rahim, A. Genc, F. H. (SAM) Froes, Phase transformation in Ti-6Al-4V-xH alloys, Met. Trans.A. 32 (2001) 2453-2463.

[5] N. Narita, C. J. Altstetter, H. K. Birnbaum, Hydrogen-related phase transformations in austenitic stainless steels, Met. Trans.A. 13 (1982) 1355-1365.

[6] V. M. Avdyukhina, G. P.Revkevich, A. Z. Nazmutdinov, G. S. Burkhanov, N. R. Roshan, N. B. Kol'chugina, Hydrogen-induced phase transformations in Pd-8.3 at. % Y alloy, Journal of Surface Investigation. 2 (2008) 429-432.

[7] C. J. Smithells, E. A. Brandes, Metals Reference Book, fifth ed., Butterworths, London, 1976.

[8] Y. Sakamoto, K. Takao, T. B. Flanagan, Hydrogen-induced suppression of ordering to Pd7M (M = Sm, Gd, Li) (Pt7Cu-type superlattice), J. Phys.: Condens. Matter. 5 (1993) 4171-4178.

[9] A. S. Darling, Some properties and applications of the platinum-group metals, Int. Met. Rev. 18 (1973) 91-122.

[10] C. H. Johannson, J. O. Linde, Röntgenographische Bestinimung der Atomanordnung in den Mischkristallreihen Au-Cu und Pd-Cu, Ann. Physik. 78 (1925) 439-460.

[11] H. Lipson, Order-disorder changes in alloys, Prog. Met. Phys. 2 (1950) 1-52.

[12] N. Kurnakov, S. Zhemchuzhniu, M. J. Zasyedatelev, Zhurnal Russkogo fiziko-khimicheskogo obshchestva pri Leningradeskom universitete, Phys. Chem. Soc. 47 (1915) 870-897.

[13] E. C. Bain, Cored crystals and metallic compounds, Chem. Met. Eng. 28 (1923) 65-69.

[14] C. S. Barrett, T. B. Massalski, Structure of Metals: Crystallographic Methods, Principles and Data, third ed., Pergamon Press, Oxford, 1980.

[15] N. S. Stoloff, R. G. Davies, The Mechanical Properties of Ordered Alloys, first ed., Pergamon Press, Oxford, 1966.

[16] E. Savitsky, V. Polyakova, N. Gorina, N. Roshina, Physical Metallurgy of Platinum Metals, Mir Publishers, Moscow, 1978.

[17] B. Welber, R. Weberer, F. Trumbore, Specific heat and energy of transformation of Mg_3Cd, Acta. Met. 1 (1953) 374-376.

[18] R. G. Davies, N. S. Stoloff, Mechanical properties and superlattice formation of Mg_3Cd, Trans. Amer. Inst. Met. Engrs. 230 (1964) 390.

[19] R. H. Taylor, S. Curtarolo, G. L. W. Hart, Predictions of the Pt_8Ti phase in unexpected systems, J. AM. Chem. Soc. 132 (2010) 6851-6854.

[20] G. Corbel, M. Topic, A. Gibaud, C. I. Lang, Selective dry oxidation of the ordered Pt-11.1 at. % V alloy surface evidenced by in situ temperature-controlled X-ray diffraction, J. of Alloys and Compds. 509 (2011) 6532-6538.

[21] S. Nxumalo, C. I. Lang, Thermodynamic stability of Pt_8V, J. Alloys and Compds. 425 (2006) 181-184.

[22] W. E. Quist, C. J. van der Wekken, R. Taggart, D. H. Polonis, Intermediate compound Ni_8Nb(Cb) in nickel-rich nickel-niobium (columbium) alloys, Trans. AIME. 245 (1969) 345-349.

[23] P. Pietrokowsky, Crystallography: novel ordered phase, Nature, 206 (1965) 291.

[24] D. Schryvers, S. Amelinckx, The ordering phenomena in Pt_xTi and Pt_xV ($3 \leq x \leq 8$) Studied by electron difraction and high resolution electron microscopy, Res Mech. 22 (1987) 101-149.

[25] P. Krautwasser, S. Bhan, K. Schubert, Strukturuntersuchungen in den Systemen Ti-Pd und Ti-Pt, Z. Metallk. 59 (1968) 724-729.

[26] P. J. Meschter W. L. Worrell, An investigation of high temperature thermodynamic properties in the Pt-Zr and Pt-Hf systems, Met. Trans. A. 8 (1977) 503-509.

[27] E. G. Kendall, C. Hays, R. E. Swift, The zirconium-platinum alloy system, Trans. Metall. Soc. AIME. 22 (1961) 445-451.

[28] G. B. Fairbank, C. J. Humphreys, A. Kelly, C. N. Jones, Ultra-high temperature intermetallics for the third millennium, Intermetallics. 8 (2000) 1091-1100.

[29] A. Raman, K. Schubert, Strukturuntersuchungen in einigen zu T^4-T^9 homologen und quasihomologen Legierungssystemen, Z. Metallk. 55 (1964) 704-710.

[30] J. K. Stalick, R. M. Waterstrat, The zirconium-platinum phase diagram, J. of Alloys and Compds. 430 (2007) 123-131.

[31] R. M. Waterstrat, The vanadium-platinum constitution diagram, Met. Trans. 4 (1973) 455-466.

[32] D. Shryvers, J. Van Landuyt, S. Amelinckx, Electron microscopy study of a new ordered phase in the platinum-vanadium (8 : 1) system, Mat. Res. Bull. 18 (1983) 1369-1374.

[33] W. Pfeiler, B. Sprusil, Atomic ordering in alloys: stable states and kinetics, Mater. Sci. Eng.A. 324, (2002) 34-42.

[34] D. A. Porter, K. E. Easterling, Phase Transformations in Metals and Alloys, second ed., Chapman & Hall, London, 1981.

[35] P. Feltham, Grain growth in metals, Acta Metall. 5 (1957) 97-105.

[36] S. Nxumalo, The Pt_8V Ordering Transformation in pt 11 at. % v, PhD thesis, University of Cape Town, 2006.

[37] J. L. Goldstein, D. E. Newbury, P. Echlin, D. C. Joy, A. D. Romig, C. E. Lyman, C. Fiori and E. Lifshin, Scanning Electron Microscopy and X-Ray Microanalysis: A Text for Biologists, Materials Scientists, and Geologists, second ed., Kluwer Academic/Plenum Publishers, second ed., New York, 1992.

[38] S-K. Kang, J-Y. Kim, C-P. Park, H-U. Kim and D. Kwon, Convetional Vickers and True Instrumented Indentation Tests, J. Mater. Res. 25 (2010) 337-343.

[39] A. Nayar, Testing of Metals, Tata McGraw-Hill Publishing, 2005.

[40] M. P. Nzula, Order Hardening in Platinum Chromium Alloys, PhD thesis, University of Cape Town, 2004.

[41] R. G. Henning, D. R. Trinkle, J. Bouchet, S.G. Srinivasan, R. C. Albers and J.W. Wilkins, Impurities Block the α to ω Martensite Transformation in Titanium, Nature Materials, 4 (2005) 129-133.

[42] D. C. Jacobson, J. M. Poate and G. L. Olson, Zone Refining and Enhancement of Solid Phase Epitaxial Growth Rates in Au-implanted Amorphous Si, Journals and Magazines, 42 (1986) 118-120.

[43] I. Baker, Recovery, Recrystallization and Grain Growth in Ordered Alloys, Intermetallics, 8 (2000) 1183-1196.